PRESSURE SENSING WITH FIBER

OPTICS AND INTERFEROMETRY

THESIS

AFIT/GE/EE/81M-7   EDDIE J. PRESTON

2LT   USAF

DTIC

JUL 1 1981

PRESSURE SENSING WITH FIBER OPTICS

AND INTERFEROMETRY

THESIS

Presented to the Faculty of the School of Engineering

of the Air Force Institute of Technology

Air University

In Partial Fullfillment of the

Requirements for the Degree of

Master of Science

by

EDDIE J. PRESTON

2LT   USAF

Graduate Electrical Engineering

December 1980

Preface

The purpose of this thesis was to examine the concept of pressure measurement with fiber optics and interferometry, to build a working prototype, and to test that prototype. Some consideration was given toward the use of the transducer system for taking intravascular blood pressure readings.

The prototype was designed to exibit the feasibility of the pressure measurement technique and little time remained for the optimization of system parameters. I beleive that significant improvements are possible now that the primary noise sources have been identified.

Table of Contents

iv

List of Figures

List of Tables

List of Symbols

Amp	Amplifier
A/O	Acousto-optic modulator
A_f, A_s	Area fiber core, source
A_1, A_2	Wave amplitude
BS	Beam splitter
c	Speed of light
$^\circ$C	Degrees centigrade
Comp.	Compensation circuit
cm Hg	Centimeters of mercury
c_{11}, c_{12}, c_{44}	Material constant
d	Laser cavity length
D	Optical path difference
d_f	Depth of focus
E	Young's modulus
$E_{c(max)}$	Maximum coupling efficency
$E_{(111)}$	Young's modulus for the (111) plane
E_T	Total electric feild intensity
$E_1(r,t)$, $E_2(r,t)$	Linearly polarized wave feild intensity
e_1, e_2	Initial wave phase
FSR	Free spectral range
f_k	Laser frequency plus A/O center frequency
f_1	Lens focal length
f_m	Modulation frequency

f_t	Total laser frequency after modulation
Δf	Laser linewidth
Δf	VCO FM modulation range
HVA	High voltage amplifier
Hz	Hertz
I	Intensity or irradiance per application
I_1, I_2	Irradiance due to respective waves
I_{12}	Interference term irradiance
I_o	Initial irradiance
I_{max}	Maximum photodiode irradiance
KHz	Kilohertz
K(s)	System transfer function
$K_1 \cdot r$	Plane perpendicular to K_1 vector
l, L_1	Length of PZT branch of interferometer
L, L_2	Length of sensing branch of interferometer
LIA	Lock-in amplifier
l_c	Coherence length
L_f	Optical path length within fiber
L_n	Path length with index of refraction accounted for
L_r	Resonant cavity length
ΔL	Change in optical path length
mm	Millimeter
mmHg	Millimeter of mercury (pressure)
n	Index of refraction
n	Constant

NA	Numerical aperature
N_{Comp}	Compensation circuit noise
N_{HVA}	High voltage amplifier noise
N_I	Stray intensity noise
N_L	Length variation noise
N_{LIA}	Lock-in amplifier noise
N_P	Pressure deviation noise
N_{PZT}	PZT noise
P	Pressure
ΔP	Change in pressure
δP	Differential pressure
PZT	Piezoelectric length transducer
r	Distance from diaphragm center
R	Diaphragm radius
s_{11}, s_{12}, s_{44}	Material constant
SNR	Signal to noise ratio
t	time
t	Diaphragm thickness
u	Poisson's ratio
$u_{(111)}$	Poisson's ratio in (111) plane
V	volts
V_I	Detector output voltage
V_m	Modulation frequency voltage level
V_o	Phase detector output voltage
VCO	Voltage controlled oscillator

WBPA	Wide band power amplifier
θ	Angle
θ_d	Detected phase with noise
$\Delta\theta_d$	Detected phase without noise
θ_e	Error signal
θ_o	Initial phase
θ_p	Pressure phase with nonlinearities
$\delta\theta_p$	Phase change due to pressure
$\delta\theta$	Correction phase from control system
λ	Wavelength
λ_k	Wavelength due to f_k
λ_t	Wavelength due to f_t
$\Delta\lambda$	Change in wavelength
μ	Microns
ω	Angular frequency
ω_i	Initial beam radius
ω_o	Focused beam waist
ΣAmp	Summing amplifier
$< >$	Time average of enclosed quantity

Abstract

A new pressure sensing device has been analyzed, built, and tested. The device uses a Michelson interferometer to monitor pressure-induced fluctuations of a polished silicon diaphragm. Probe flexibility is achieved by mounting the diaphragm on the end of a single mode optical fiber; the coupling apparatus used permits interference to occur with the fiber in one leg of the interferometer. The phase of the resulting pattern is locked using a piezoelectric length transducer and phaselock loop control techniques.

Formulas developed to model the system input/output characteristics led to the construction of a working prototype. Long term drift for the system was negligible. Short term drift limited the resolution of the system to 7 mmHg over the region 50 mmHg to 200 mmHg. The limited range resulted from the scanning limit of the piezoelectric length transducer. System linearity was approximately 5 percent. Computer noise analysis identified the high voltage DC amplifier and the piezoelectric length transducer as limiting resolution to 3 mmHg.

Acousto-optic modulation was examined as an alternative control method. This approach offers better resolution and better frequency response.

The performance of the prototype pressure sensing system suggests that state-of-the-art specifications could be achieved by this method. Application for intravascular blood pressure measurement is discussed.

xii

I. Introduction

Background

Since the conception of pressure and its measurement by Torricelli in 1643, inventors have gone to great lengths to extract useful information from this mechanical principle. Many devices have been constructed whose sole purpose is to convert fluid pressure or fluid flow into an electrical signal containing the same information. These transducers have taken many forms. Most modern electronic sensors use a physical principle to monitor the motion of a flexing diaphragm.

Electronic pressure sensors use many different physical properties to accomplish their task. Strain gages use a Wheatstone bridge circuit to monitor the motion of an armature that is directly connected to a flexing diaphragm. Capacitive transducers measure the changing capacitance between two plates as the separation between them changes. One plate is attached to a diaphragm. Inductive transducers measure the changing flux caused by a magnetic disc attached to a diaphragm as the disc moves relative to a stationary coil. Piezoelectricity and piezoresistivity rely on the changing electrical properties of a crystal as mechanical stress or pressure is applied. Other principles that have been used are P-N junctions, variable light reflectivity, resonant wire, and magnetostriction. The diversity of approaches to the pressure measurement problem hints at the significance of the information that the devices gather.

Current pressure sensors meet the demands of diverse applications

with varying degrees of success. Many applications such as in-vivo cardiovascular pressure measurement have strict design criteria that eliminate most sensors from consideration. This application is analyzed in depth in Appendix E. The principle behind the fiber optic pressure transducer offers significant possibilites for meeting these criteria.

The use of a Michelson interferometer to measure the motion of the diaphragm permits accurate measurement of small fluctuations. The addition of an optical fiber furnishes probe flexibility and probe size limited only by diaphragm characteristics. A very small diaphragm can be etched from a silicon wafer and mounted to the fiber end. The short term drift encountered during the experiment limited resolution to 7 mmHg. Noise from the piezoelectric length transducer (PZT) and the associated high voltage DC amplifier were found to limit resolution to 3 mmHg. Indicating that both problems must be solved before a reliable pressure sensing system can be constructed.

The originality of this thesis arises from a new combination of existing technologies to create a potentially useful pressure sensing device. Although this research was conducted with the cardiovascular pressure sensing application in mind, many other applications are possible.

Problem Statement

The problem addressed in this thesis is to determine the feasibility of the fiber optic pressure measurement technique. This includes identification and analysis of problem ares, design and construction of a prototype, testing, and error analysis. Determination of suit-

ability for the biomedical application per the criteria in Appendix E leads to the commentary on system value and on continued research.

Research Approach

Analysis of the fiber optic pressure transducer system began with derivation of system equations to determine if the concept was sound. This led to experimentation with optical fibers and phaselock control techniques. It was shown that light could make the round trip through the single mode fiber with output power levels that were detectable by a photodiode. Phaselock was achieved with the compensation circuit shown in Appendix D. These results indicated that the system could function properly.

The interferometer was constructed and locked before the fiber was introduced into the system. Alignment problems associated with the small core single mode fiber were worked out with changes in mounting hardware. The system was then locked with the fiber in place and prepared for testing with steps to reduce the noise level.

Testing for drift, linearity, resolution, and noise characteristics was completed. Analysis of the results led to the conclusions and recommendations shown in Chapter Five.

Chapter Two contains theory pertaining to the operation of the fiber optic pressure sensor. Chapter Three contains a description of system operation. Chapter Four contains the experimental procedure and the results obtained. The experiment is concluded in Chapter Five with conclusions and recommendations.

II. Theory

Introduction

The Michelson interferometer offers very accurate measurement of small length fluctuations by the property of light interference. (Ref 11:290) The output intensity of the interferometer is dependent upon the change in path length (ΔL) of the active branch compared to the reference branch. This length change can be developed by applying pressure to a flexible diaphragm mirror in the active branch. Analysis of the relation between pressure and length fluctuations results in the desired pressure measurement capability. An optical fiber can be placed in the active branch to obtain a flexible probe that can be taken to the pressure source. The small etched diaphragm is mounted on the fiber end. The system offers some unique possibilities for special application sensing.

Michelson Interferometer

Two plane waves interfere in the Michelson interferometer to give an output intensity pattern that varies with changes in optical path length of the active branch. The interference phenomenon can best be understood by examining the wave nature of light and then applying the superposition principle. The general equation of a linearly polarized wave is given below.

$$E_1(r,t) = A_1 \cos (K_1 \cdot r - \omega t + e_1) \qquad \text{(Eq. 2.1)}$$

where:

A_1 = amplitude $\qquad\qquad$ ωt = angular frequency $\cdot$ time

$K_1 \cdot r$ = plane $\perp$ to K_1 vector $\qquad$ e_1 = initial wave phase

4

Two such waves can be combined by the superposition principle to get the total electric field intensity $E_T = E_1(r,t) + E_2(r,t)$ which is merely the sum of the individual waves. Due to the high frequency of the signals being monitored the photodiode measures irradiance not field intensity. Irradiance is defined by $I = \alpha v < E_T^2 >$ where α is the permativity constant of the medium, v is the velocity in the medium and $< E_T^2 >$ is the time average of the field intensity squared. Concern with only relative irradiance within the same medium permits the medium constants to be neglected. (Ref 11:277) The irradiance can therefore be taken as $I = < E_T^2 >$ measured in watts/ meter^2. Expanding the equation yields the interference term of interest (I_{12}) as shown.

$$ I = < E_T^2 > = I_1 + I_2 + I_{12} \qquad \text{(Eq. 2.2)} $$

where
$$ I_1 = < E_1^2 > $$
$$ I_2 = < E_2^2 > $$
$$ I_{12} = < E_1 E_2 > $$

Taking the time average by the definition $< E_T > = 1/T \int_t^{t+T} E(t') \, dt'$ yields the following equation for the interference term.

$$ I_{12} = A_1 A_2 \cos (2\pi (D+\Lambda L)/\lambda) \qquad \text{(Eq. 2.3)} $$

where:
- A_1, A_2 = respective amplitudes
- D = optical path difference
- ΛL = optical path difference due to pressure
- λ = wavelength of source

Total constructive interference will occur when $\cos (\delta) = 1$. This occurs when $\delta = 0, \pm 2\pi, \pm 4\pi \dots$ Since D and λ are constant, a constructive interference peak will occur everytime ΛL changes by $\lambda/2$ in length.

These length changes are illustrated in the Michelson interferometer
of Figure 2.1.
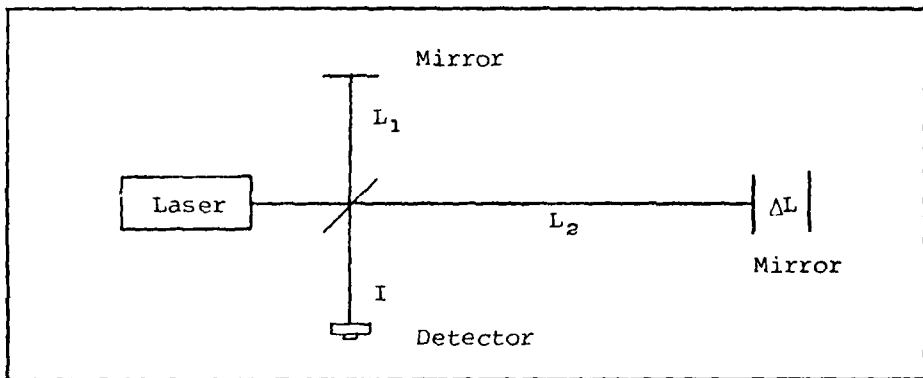
Figure 2.1 Michelson Interferometer

The change in path length (ΔL) can be produced by applying pressure to
a suitable diaphragm mirror.

Diaphragm Mechanics

Equations relating diaphragm motion to applied pressure have been
derived for many different diaphragm geometries. The generally accepted
equation for displacement of a rigidly held circular diaphragm is
shown below. (Ref 3:216)

$$\Delta L = \frac{3\,(1-u^2)\,(R^2 - r^2)^2\,\delta P}{16\,E\,t^3\,(1 + (\Delta L/t)^2/2)} \qquad (Eq.\ 2.4)$$

where: ΔL = displacement of diaphragm at radius r   (cm)
           u = Poisson's ratio   (unitless)
           E = Young's modulus   (dynes/cm^2)
           R = diaphragm radius   (cm)
           r = distance from diaphragm center   (cm)
           t = diaphragm thickness   (cm)
           δP = pressure differential   (dynes/cm^2)

6

The complexity of the equation reduces significantly if the following assumptions are made. First, assume that the area of interest on the mirror is the center (r=0). Second, assume $\Delta L < t/4$ to guarantee good diaphragm linearity characteristics (better than 1%). These two assumptions lead to the simplified equation below.

$$\Delta L = \frac{3\ (1-u^2)\ R^4\ \delta P}{16\ E\ t^3}$$

Further simplification can be achieved by calculating values for E ans u for the (111) silicon diaphragm, as shown by Runyan (Ref 27:93).

$$E_{(111)} = \frac{4}{2s_{11} + 2s_{12} + s_{44}}$$

$$u_{(111)} = 1/6\ (5s_{12} + s_{11} + s_{44}/2)\ E_{(111)}$$

where:
$$s_{11} = \frac{c_{11} + c_{12}}{(c_{11} - c_{12})\ (c_{11} + 2c_{12})} \qquad = 0.7644 \times 10^{-12}$$

$$s_{12} = \frac{- c_{12}}{(c_{11} - c_{12})\ (c_{11} + 2c_{12})} \qquad = 0.2143 \times 10^{-12}$$

$$s_{44} = 1/\ c_{44} \qquad = 1.256 \times 10^{-12}$$

Solving for E and u yields:

$$E = 1.9 \times 10^{12}$$

$$u = 0.3825 \qquad\qquad 1 - u^2 = 0.8537$$

Inserting these constants into the above equation yields:

$$\Delta L = 8.425 \times 10^{-14}\ R^4/\ t^3\ \delta P \qquad\qquad (Eq.\ 2.5)$$

Combining equations 2.2 and 2.5 yields the desired relationship

between applied pressure and the interferometer output irradiance.

$$I = I_1 + I_2 + A_1 A_2 \cos \left(2\pi \frac{D + 8.425 \times 10^{-14} R^4 / t^3 \delta P}{\lambda} \right) \quad \text{(Eq. 2.6)}$$

Therefore, if the radius-to-thickness ratio can be scaled properly the

system will measure pressure. But the usefulness of the system is

limited by the inflexibility of the pressure sensing probe. An optical

fiber can be placed in the pressure sensing branch of the interferometer

to permit the light beam to be guided to the pressure source.

Fiber Optics

The introduction of the optical fiber into the interferometer

changes some of the system characteristics. The optical path length

through the fiber is longer than the same length of air. The two

factors causing the change are the different index of refraction and

the multiple reflective path now taken by the light. The new path

length will be $L_n = n L_f$ where n is the index of refraction of the

fiber core material and L_f is the path length along the fiber. The path

length L_f is a function of the input angle to the fiber.

Another consideration brought on by the fiber is the question as

to whether sufficient coherence can be maintained to allow interference.

The phase relationship of the light wave must remain intact to be

coherent. Optical fibers that allow multiple paths for the light to

travel typically have high dispersion because each path has a different

travel time and they arrive at the output out of phase. Single mode

fibers allow only one mode to exist thus maintaining coherence. This

8

result was noted by Kapany in the original research: " For small fibers only a few permissible characteristic angles exist and an appreciable degree of coherence is attainable ". (Ref 17:54) Single mode fibers are analyzed with the laws of physical optics since the core diameters are on the order of a few wavelengths of the source radiation. An alternative to the single mode fiber is the continuous refocusing found in graded index fibers. Multiple modes are present in the fiber be due to the fiber design these modes propagate at the same speed down the fiber and arrive in phase with good coherence.

The final consideration to be discussed here concerns the need to couple the light efficently into and outof the fiber. Maximum coupling efficency is given by Liouville's theorm for statistical mechanics using conical coordinate axes. (Ref 29:34)

$$E_c(max) = A_f / A_s \sin^2\theta = A_f / A_s (NA)^2$$

where: A_f = fiber core area $\quad$ A_s = source area

θ = angular acceptance $\quad$ NA = numerical aperature

Using typical numbers for the experimental apparatus, fiber core diameter = 5 microns, laser source diameter = 1 mm, and NA = 0.18 the best coupling efficency has a loss of approximately 60 db. The obvious unacceptability of this loss results in examination of a focusing lens alternative in Chapter Four.

Each of the above sections contributes information suggesting the feasibility of the fiber optic pressure sensing technique. The operation of the system is described in Chapter Three.

III. Fiber Optic Pressure Transducer

Introduction

The fiber optic pressure transducer draws togather many existing technologies to form a unique pressure sensing device. The sensitivity of a Michelson interferometer offers high accuracy with minimal diaphragm movement. The creation of low dispersion single mode fiber brought about the transmission of light without significant degradation of coherence. A fiber can therefore be used as a probe in one leg of the interferometer. Locking the interference pattern with phaselock techniques yields a voltage output variable. The ability of this sensor is therefore limited only by the low level noise sourecs and the selection of system components.

General Description

The fiber optic pressure transducer, like most other modern electronic pressure sens devices, monitors the motion of a diaphragm flexing under a differential pressure. It differs from the others by using an interferometer as the monitoring device. The Michelson interferometer can be seen in the general system diagram of Figure 3.1. The amplitude of the laser source is split into two branches by the beam splitter. These two coherent light beams are later recombined at the photodiode to yield an interference pattern. This pattern changes when the optical path length of one interferometer branch changes relative to the other branch. Pressure changes are translated to length changes by a flexible silicon diaphragm mirror. The interference pattern achieved is shown in Figure 3.2 with a graph of center intensity

Piezoelectric Length Transducer

Beam Splitter   Optical Fiber

Laser   Lens   Mirror
                                                 Diaphragm

Photodiode

Control Loop Electronics
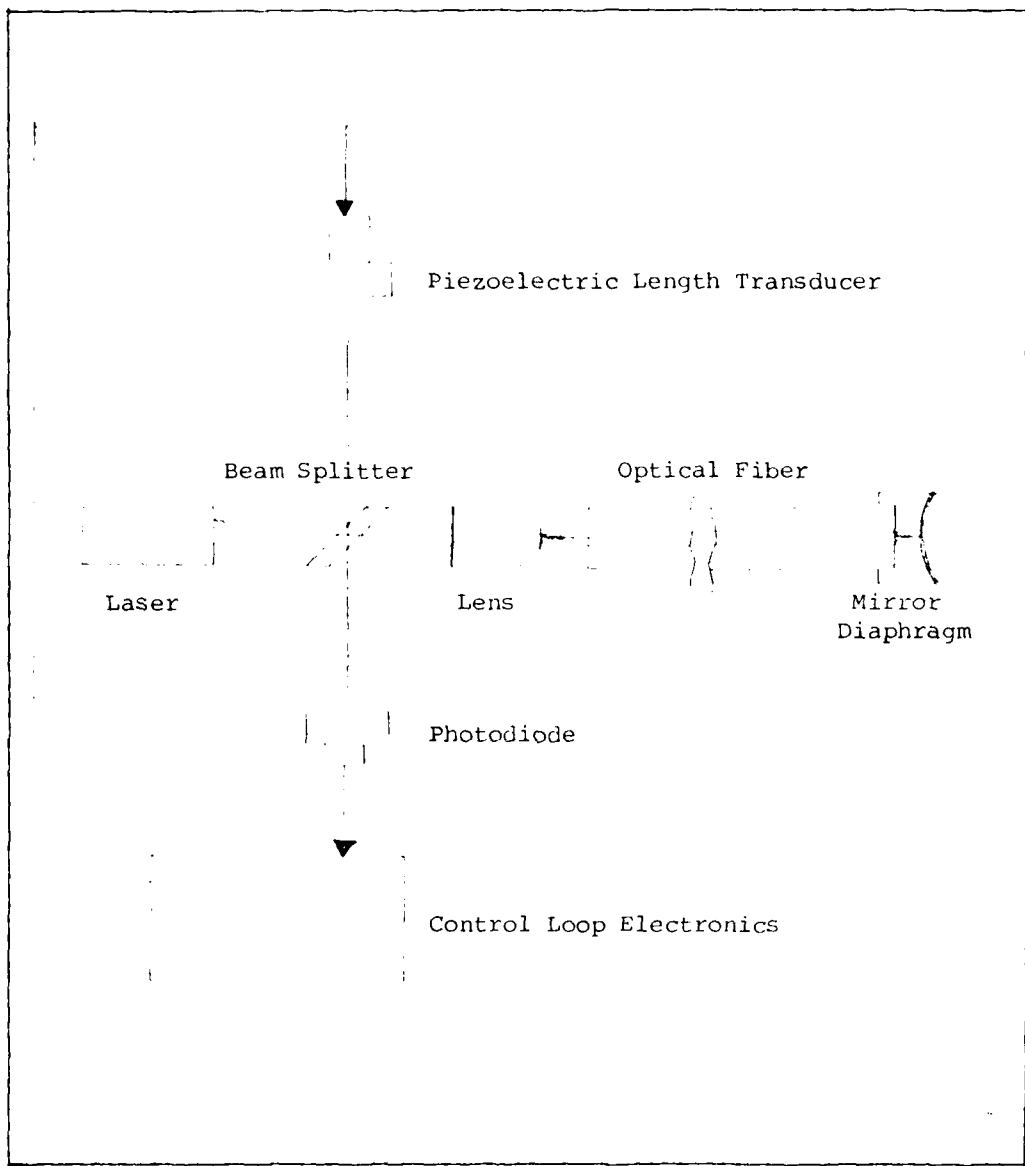
Figure 3.1   Pressure Transducer General Diagram.

11

vs. length change. An optical fiber placed in one branch of the
interferometer permits flexibility for the pressure sensing probe.
The reflective silicon diaphragm mounts on the end of the fiber which
is to be immersed into the pressure medium.
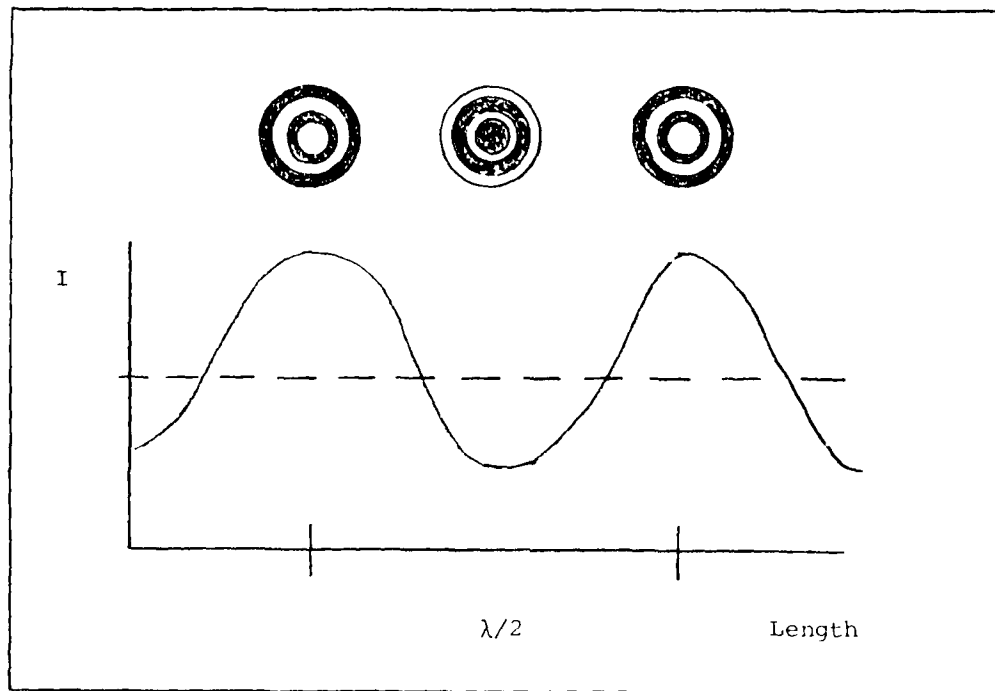
Figure 3.2 Center Intensity vs. Path Length

The control loop locks the phase of the interference pattern to
the nearest constructive peak as shown in Figure 3.2. Phase lock is
maintained by moving the reference mirror with the piezoelectric length
transducer (PZT). The reference mirror is moved the same direction and
the same distance as the diaphragm. The DC voltage applied to the PZT
changes when these corrections are made. The voltage is directly
related to the pressure and can be monitored on a chart recorder.

12

Control Analysis

The PZT control loop locks the phase relationship between the two
interferometer branches by varying the position of the PZT mounted
mirror. The system is locked to the constructive peak in Figure 3.2
by the modulation technique described in Appendix B. The quality of
the interference pattern can be described by the visibility. (Ref 11:426)
This quantity allows the degree of coherence to be measured. The phase
of the modulation signal is detected by the lock-in amplifier (LIA).
A positive error signal is developed if the optical path length (OPL)
is too long. A negative signal is developed if the OPL is too short.
This error signal is low pass filtered and sent to the high voltage
amplifier (HVA) to correct the PZT positioning of the mirror. A general
diagram of control loop operation is shown in Figure 3.3.

Explanation of control functions is simplified by the control
diagram in Figure 3.4. The condition for the desired phase lock to
occur is that the control loop correction phase $\delta\theta$ must be equal and
opposite to the phase change due to the applied pressure $\Delta\theta_p$. The error
signal θ_e guarantees that this will occur as explained above. The phase
correction is given by the following equation.

$$\delta\theta = K(s) \, (\, \theta_d - \Delta\theta_p - \theta_o - \delta\theta \,)$$
$$= \frac{K(s)}{1+K(s)} \, [\, (\, \theta_d - \theta_o \,) - \Delta\theta_p \,]$$

Analysis of the above equation shows that the error signal θ_e will be
cancelled out if it is entirely due to the applied pressure. This
analysis changes when noise sources are considered. These will be
discussed in the next section.

Photodiode

I_O

ΛL

Laser

PZT

HVA

Lock-In
Amplifier

f_m

Compensation
Network
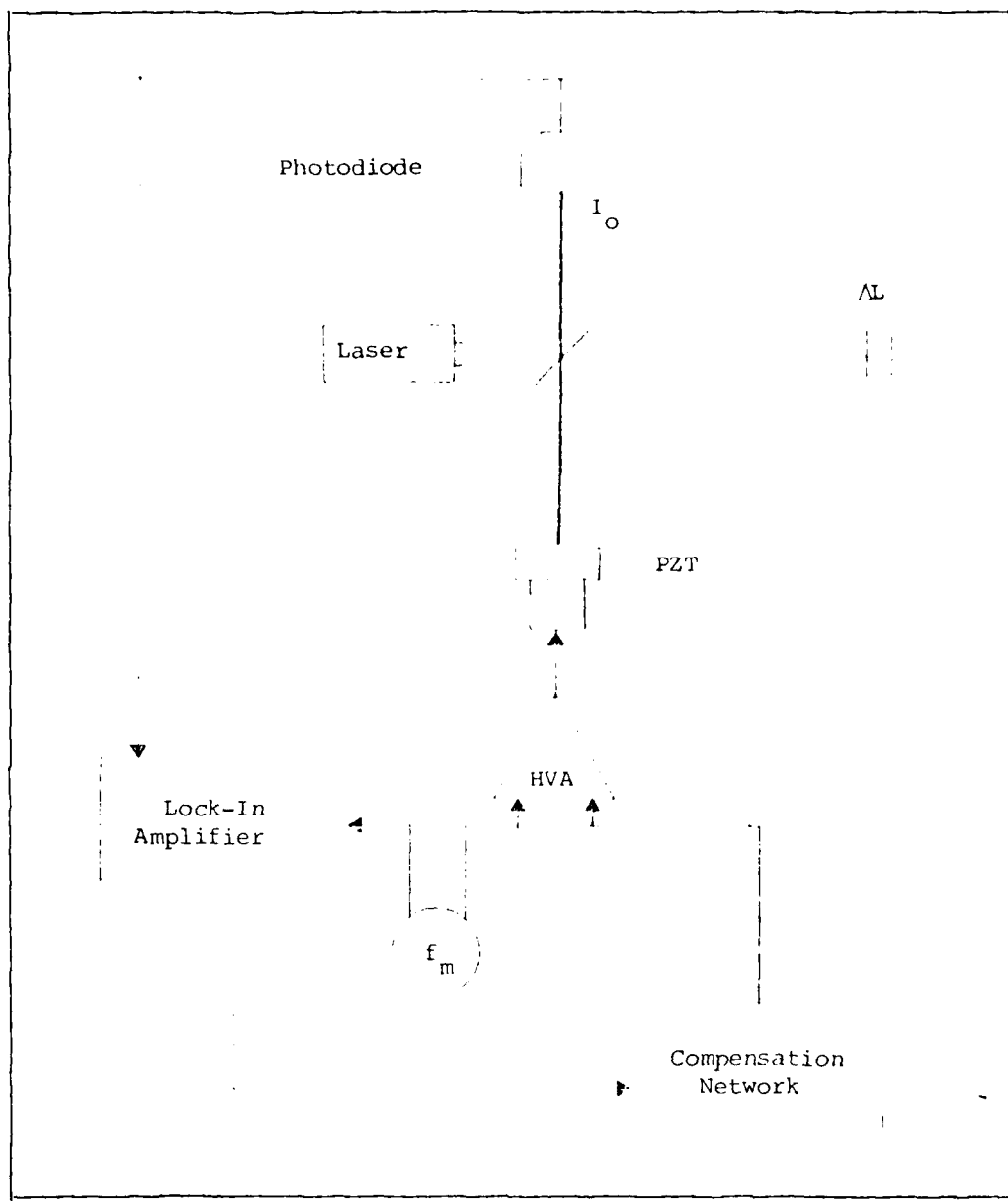
Figure 3.3   PZT Control Loop Operation.

14

$$\theta_d \xrightarrow{\quad +\quad} \bigcirc \xrightarrow{\quad \theta_e \quad} \boxed{K(s)}$$

$$\delta\theta_p \xrightarrow{\quad +\quad} \bigcirc \xleftarrow{\quad +\quad \delta\theta \quad}$$

$$\theta_o$$
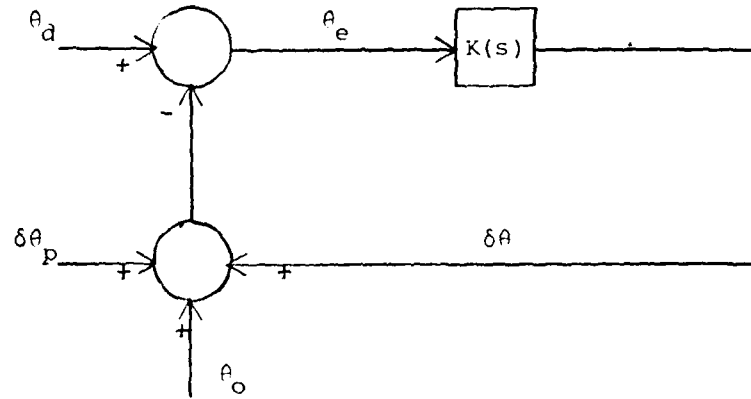
|		
θ_d	=	Detected phase
θ_e	=	Error signal
θ_o	=	Initial loop phase
$\delta\theta$	=	Correction phase
$\delta\theta_p$	=	Phase change due to pressure
$K(s)$	=	Loop transfer function

Figure 3.4   Control Loop Diagram

Error Analysis

The degree to which errors can be controlled determines the limitations on system accuracy and system resolution. All identified errors have been listed in Table 3.1. Some of these errors are analyzed experimentally in Chapter Four. The errors can be broken down into four groups, each representing a physical variable, length, intensity, pressure, and electrical noise.

Changes in the optical path length ΔL can arise from a number of sources. Variations in temperature can cause thermal expansion of the mounting plate and air movement in the surrounding area. Vibrations can cause slight changes in length. PZT jitter due to the modulation technique employed is another source of length variation.

Undesired changes in light intensity impinging on the photodiode can raise noise levels. Light from extraneous sources should be eliminated, but some reflected or refracted light from the apparatus is likely to occur. Additional interference patterns can develop from light reflected from lenses or fiber faces.

Nonlinear scale factors for the diaphragm or the PZT taint the results. These nonlinearities can arise from improper mounting or improper selection of components. Some nonlinearity will always be present, and it must be accounted for in the system specifications.

Electronic noise added by control circuitry, power supplies, and amplifiers can easily be the limiting factor which determines resolution. Noise from the photodiode and its amplifier are included here. All of the above stated error sources are shown in control diagram format in Figure 3.5.

16

N_L	–	Temperature, Vibrations, PZT Jitter
N_I	–	Reflected or other Stray Light
N_p	–	Pressure Variation from Nonlinearity
N_{LIA}	–	Lock-in Amplifier
$N_{Comp.}$	–	Compensation Network
N_{HVA}	–	High Voltage Amplifier
N_{PZT}	–	Piezoelectric Length Transducer
$\Delta\theta_d$	–	Detected Phase before Noise
θ_d	–	Detected Phase with Noise
θ_e	–	Error Signal
$\delta\theta$	–	Correction Phase
$\delta\theta_p$	–	Phase Change due to Pressure
θ_p	–	Pressure Phase with Nonlinearity
θ_o	–	Initial Phase

Table 3.1   Error Sources and Terms
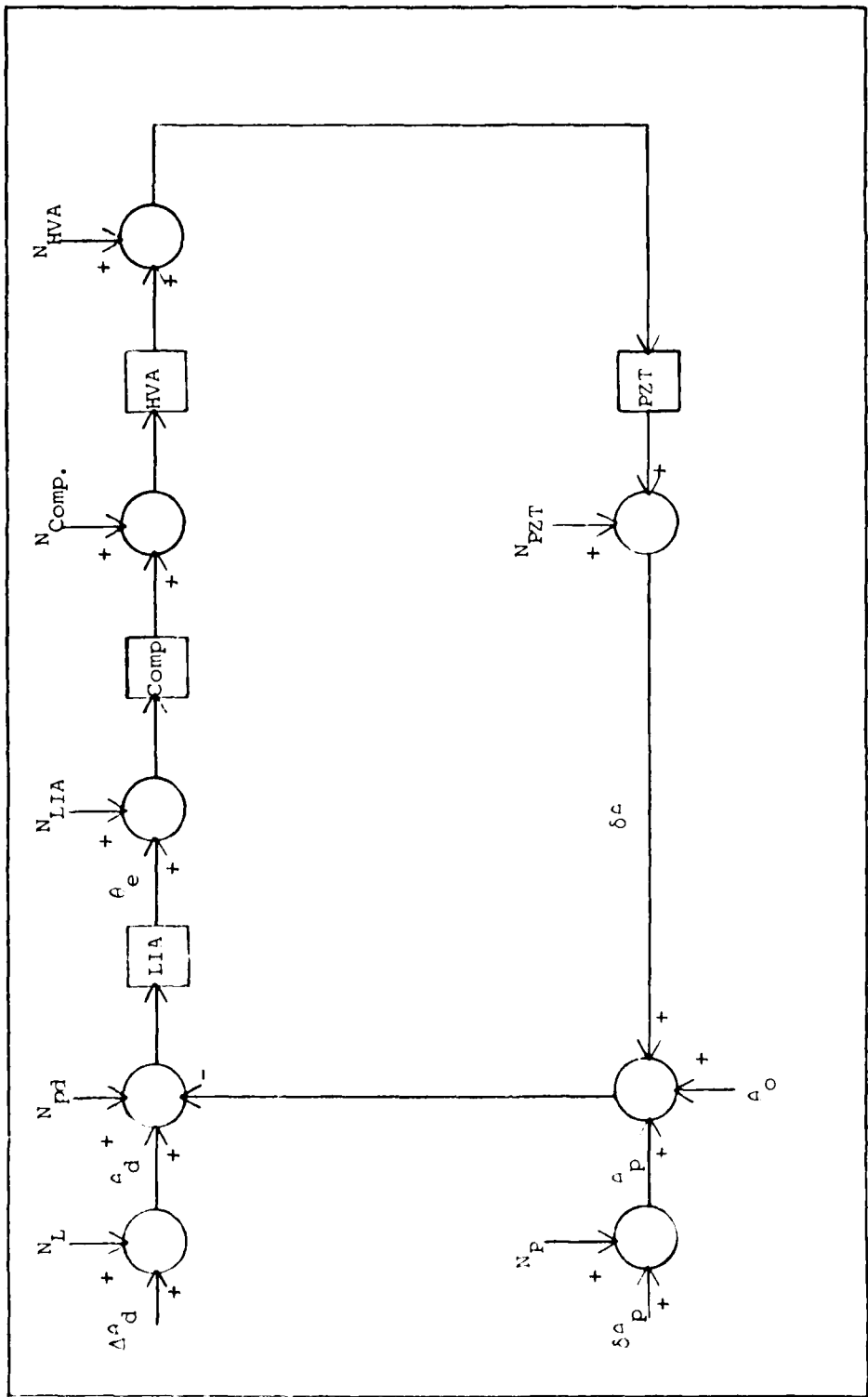
Figure 3.5 Error Analysis Control Diagram

18

Laser Selection

Proper selection of a coherent light source plays a significant role in determining the usefulness and the versatility of the fiber optic pressure transducer. Coherence length is the primary criterion for source selection because it determines the maximum usable length of the fiber sensing probe. Coherence length is given by $l_c = c/\Delta f$ (Ref 25:32) where c is the speed of light and Δf is the laser linewidth. The effective linewidth is increased significantly if more than one mode falls within the gain curve of the laser. This condition is known as multimode operation and is common in most laboratory lasers. Techniques do exist to limit a laser to single mode operation. The term single mode is taken in this report to mean only one transverse electromagnetic mode and only one longitudinal mode. The difference in linewidth for these two laser types is displayed in Figure 3.6.
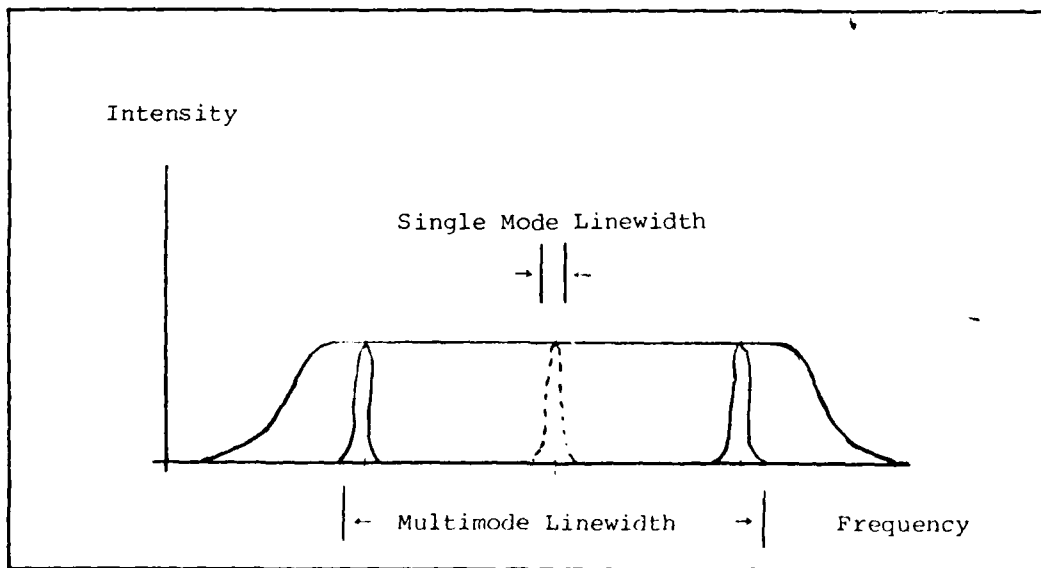
Figure 3.6 Laser Linewidths for Single and Multimode.

The effective linewidth for the HeNe laser used in this research was measured to be 800 MHz with a Fabry-Perot interferometric spectrum analyzer. This yields a coherence length of only 37.5 cm. The value was then confirmed with the experimental apparatus. The interference pattern disappeared when the above value was exceeded. To extend the coherence length, as would be needed for most applications, a single mode laser must be used.

The single mode laser offers significant improvement in coherence length by reducing the laser linewidth. A single longitudinal mode can be achieved by choosing the cavity length of the laser short enough so that the free spectral range (FSR) is wider than the gain curve of the laser. Calculation of FSR, $FSR = c/2d$ where d is the laser cavity length, indicates the necessity to keep d less than 18 cm. (Ref 11:311) Other methods exist to achieve single mode operation. Coherence lengths in excess of a kilometer can be achieved.

Fiber Optics and Hardware

Single mode fiber was selected to achieve the desired coherence necessary for interference. With this fiber come coupling problems due to the small core diameter. The problems were overcome using focusing optics and a translation stage fiber holder. The specifications for the single mode fiber used for testing are given in Table 3.2. (Ref 13:22)

core diameter	– 5.8 μ	numerical aperature	– 0.18
cladding diameter	– 111 μ	attenuation	– 7.7 db/Km
coating diameter	– 200 μ		

Table 3.2 Valtec Fiber Data (BF-SM-632).

20

In the single mode fiber the core diameter is significantly smaller than the laser spot size. Therefore some sort of focusing device must be employed to achieve maximum coupling efficency. The conical acceptance angle discussed in Chapter Two is known to decrease for smaller core diameters. Numerical aperture is a convenient method to express acceptance angle: $NA = n_o \sin \theta$. (Ref 11:151)

From diffraction theory, it can be shown that the HeNe laser used can be focused to a spot size w_o. (Ref 25:247) The following equation assumes that the beam is smaller than the lens and it gives a good approximation of actual spot size.

$$w_o = \frac{\lambda f_1}{\pi w_i} \qquad (Eq. 3.2)$$

where:

w_o = focused beam radius

w_i = initial beam radius

λ = laser wavelength

f_1 = focal length of lens

Substituting typical values into the equation: $w_i = .5mm$, $f_1 = 1$ cm, and $\lambda = 0.6328 \mu$ yields a value of $w_o = 2 \mu$. Returning to (Eq. 2.7) shows that the coupling loss has been reduced from 60 db to approximately 13 db. Further improvement could be made by decreasing the spot size even more. This can be done by increasing the magnification power of the lens and thereby decreasing the focal length. The problem here is that when the focal length is reduced, so is the distance over which the spot remains focused. The depth of focus must remain greater than the sensitivity of the fiber translator or the alignment will be nearly impossible. The z-axis sensitivity of the NGF FP-1 translator used was determined to be approximately 10 μ from experiment.

The equation for depth of focus is shown below. (Ref 25:248)

$$d_f = \frac{2\pi}{\lambda} (p - 1)^{1/2} w_o^2 \qquad \text{(Eq. 3.3)}$$

where:

d_f = depth of focus

w_o = focused beam radius

p = tolerance factor

Substituting typical values into the equation: $w_o = 2\ \mu$, $p = 1.1$ and $\lambda = 0.6328\ \mu$ gives a depth of focus $d_f = 12.5\ \mu$. The value is satisfactory, but if the magnification factor is increased to 20x the depth of focus decreases to $4\ \mu$. If any increases in signal to noise ratio are to be achieved by improvement in fiber couplig the fiber translator must be made more sensitive.

Diaphragm Characteristics

Desired properties such as flexibility and high reflectivity significantly narrow the choice of materials from which the diaphragm can be made. Silicon has these and many other suitable characteristics. Silicon is rugged, flexible, chemically inert, readily available, inexpensive, easily etched to the correct thickness, and it has good reflectivity in the HeNe laser frequency range without the use of thin film coatings. The rflectivity of the wafers used was measured to be 80 % ± 2 %.

The fiber optic pressure transducer system was built and aligned. Each component performed as was expected to yield the results shown from experimentation in the following chapter.

IV. Experiment

Procedures

Proper system operation can be achieved if careful optics alignment, meticulous fiber preparation, and careful electronics setup is followed. The alignment of system optics is straightforward as indicated in Figure 3.1. The Michelson interferometer must be set up so that the two final beams interfere as indicated by the pattern in Figure 3.2. Care must be taken to insure that lenses are centered on the laser beam. The challenge occurs when the fiber is prepared and aligned to permit coherent light to travel its length in both directions. Coupling light into the single mode fiber core requires exact adjustment. Once the interference pattern is achieved, the control loop must be adjusted and locked before data can be taken.

Fiber Preparation. The fiber coating must be stripped so that the fiber ends can be cleaved and mounted. The fiber can then be aligned at both ends to get the output beam.

Extreme care is necessary when handling optical fibers. The durability and relative insensitivity to damage changes drastically when the fiber jacket is removed. The glass fiber is especially sensitive to bending motions while rigidly held in the fiber mount. The fiber jacket can be removed mechanically with a scalpel or chemically with acids or other solvents. The jacket material determines which method yields the best result. Multiple peeling motions with the scalpel worked very well with the Valtec single mode fiber used.

The fiber face must be cleaved to get a flat perpendicular surface over the core area to aide in coupling. This can be accomplished in the following manner. Place the partially stripped fiber into a groove in the holding block. Put a plate over the fiber up to the point where the cleave is to be made. Scribe a line on the fiber with a sharp scalpel blade. These blades can be used only a few times before they get too dull to be effective. Move the fiber to the edge of the block and break the fiber at the scribed line. This method often yields an acceptable cleave. The fiber must be tested and the procedure must be repeated if the cleave is not good.

The easiest method for determining the quality of the cleave is to mount the fiber and view the output pattern. If an acceptible uniform break was acheived the pattern will be circular. With a nonuniform break the pattern is obviously not circular. When both ends have been cleaved and the mount is correctly adjusted so that the beam is focused completely into the fiber core a distinctive diffused circular pattern is observable. Index matching fluid must be used to eliminate the cladding modes to obtain the proper output pattern. It takes patience and great care to set the fiber up correctly. The fiber must be shown extreme care from this point on or the procedure will be repeated after each careless act.

The fiber should be mounted firmly in the translation holder to prevent movement. The fiber face is placed at the focal point of the focusing lens. This can be determined by insuring that the reflected output does not go through a focal point on the way to the photodiode target.

The output of the fiber can be peaked by aligning the translation stage holding the fiber. After this is done the loose fiber end can be attached to the diaphragm mounting apparatus. The mount holds the fiber face close to the flexing diaphragm without touching the diaphragm. The fiber must be as close as possible to reduce losses due to beam expansion. The intensity of the interference pattern can now be set to a maximum by fine adjustments on the diaphragm mount and on the mount holding the PZT mounted mirror.

Control Loop Adjustment. The control loop can be adjusted and locked after a high intensity interference pattern is achieved. The procedure for setting up the control loop is described below.

Step 1: Identify a PZT resonance frequency where a maximum lock-in amplifier output is attainable. This can be done by scanning the HVA with the scope horizontal output to yield a sinusoidal wave as shown in Figure 3.2. Now, scan the modulation frequency range of the lock-in amplifier to attain a good signal, .76 volts peak to peak was attained with a 0.4 volt photodiode signal. The frequency selected for the equipment used was 2.85 KHz.

Step 2: Set the lock-in amplifier to maximize the signal and to minimize the noise. The phase on the lock-in amplifier should be adjusted so that there is a 90 degree phase shift between the photodiode and LIA signals. Some care should be used to insure that the system locks to a constructive interference peak. Finally, the filter on the LIA can be adjusted to minimize the noise while not affecting the desired signal.

Step 3: Null the integrator in the compensation circuit and set

25

the gain to be within the range of the HVA. If this is not done the HVA will reset or blow a fuse depending on the position of the remaining switches.

Step 4: Connect the integrator to the summing amplifier input. If the gain knobs are set correctly the system will lock. If the phase is set correctly the lock will occur on a constructive peak. This insures a better signal to noise ratio.

Measurement Procedures. Two types of data were taken on the pressure measuring system. The output voltage of the HVA was monitored on a chart recorder under different conditions to yield information about drift, linearity, pressure range, and resolution. The output of each electronic component was connected to a noise analysis computer to yield useful information about limiting noise sources. The equipment used for this analysis is described in Appendix C.

Results

The drift characteristics of the system can be seen from the chart recorder strip in Figure 4.1. The strip represents the output of the system while it was locked for a period of 15 minutes. The long term drift is negligible. The short term drift ranges as high as 20 volts. The drift characteristics are very susceptible to motion within the test environment. Thermal considerations are also a key factor causing drift. The system was allowed to warm up for six hours before this data was taken. Further warming time did not seem to affect the results. A plexiglass cover was designed to help reduce air motion and quick thermal variations.
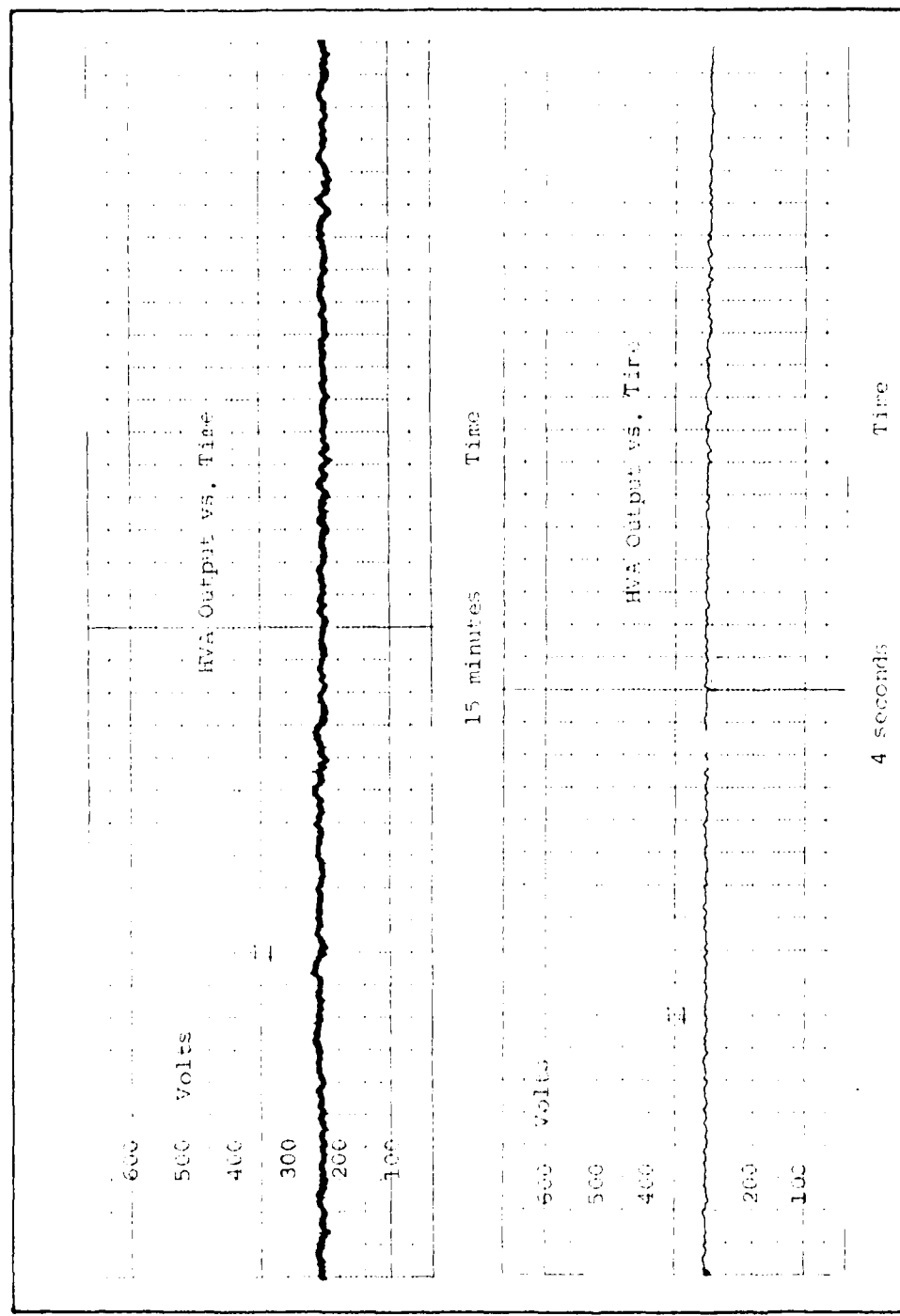
Figure 4.1   Drift Data and Noise Data.

The noise level on the second chart recorder strip in Figure 4.1 indicates that the resolution of the system is approximately 10 volts. This strip was run at 50 mm/sec., so the strip represents 4 seconds. The resolution can also be expressed in the minimum length change observable. The scale factor between voltage and PZT motion was determined by locking the system on five consecutive peaks as seen in Figure 4.2. It is known that total constructive interference occurs every half wavelength. Therefore, the PZT moves the mirror a half wavelength for each 100 volts applied to it by the HVA. This implies a resolution of 0.03 microns or 1/20 of a wavelength.
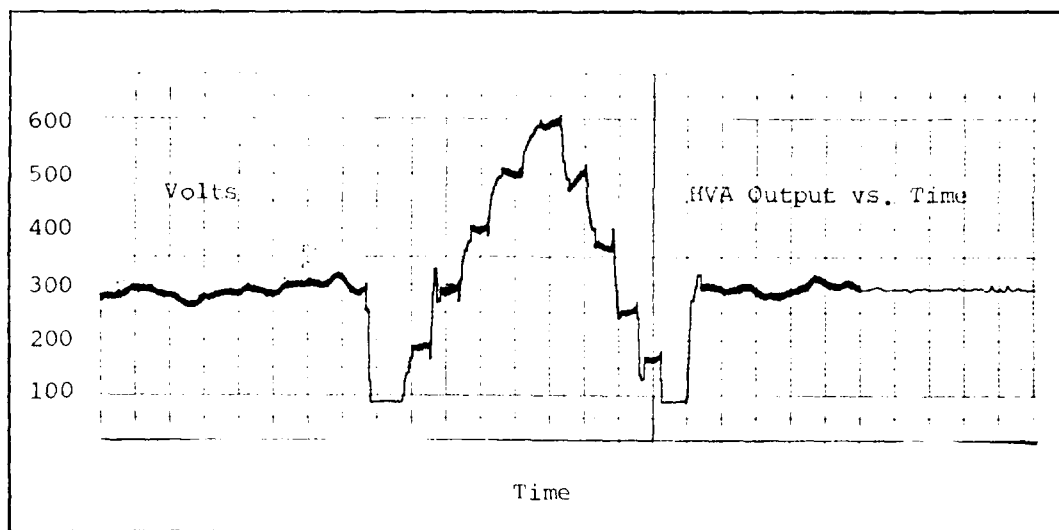
Figure 4.2 System Locked to Different Peaks.

Figure 4.2 also indicates that no large nonlinearities exist for the PZT over the range of measurement. The separation of the peaks appears to be 100 ± 5 volts.

Pressure (cmHg)

Pressure (cmHg)
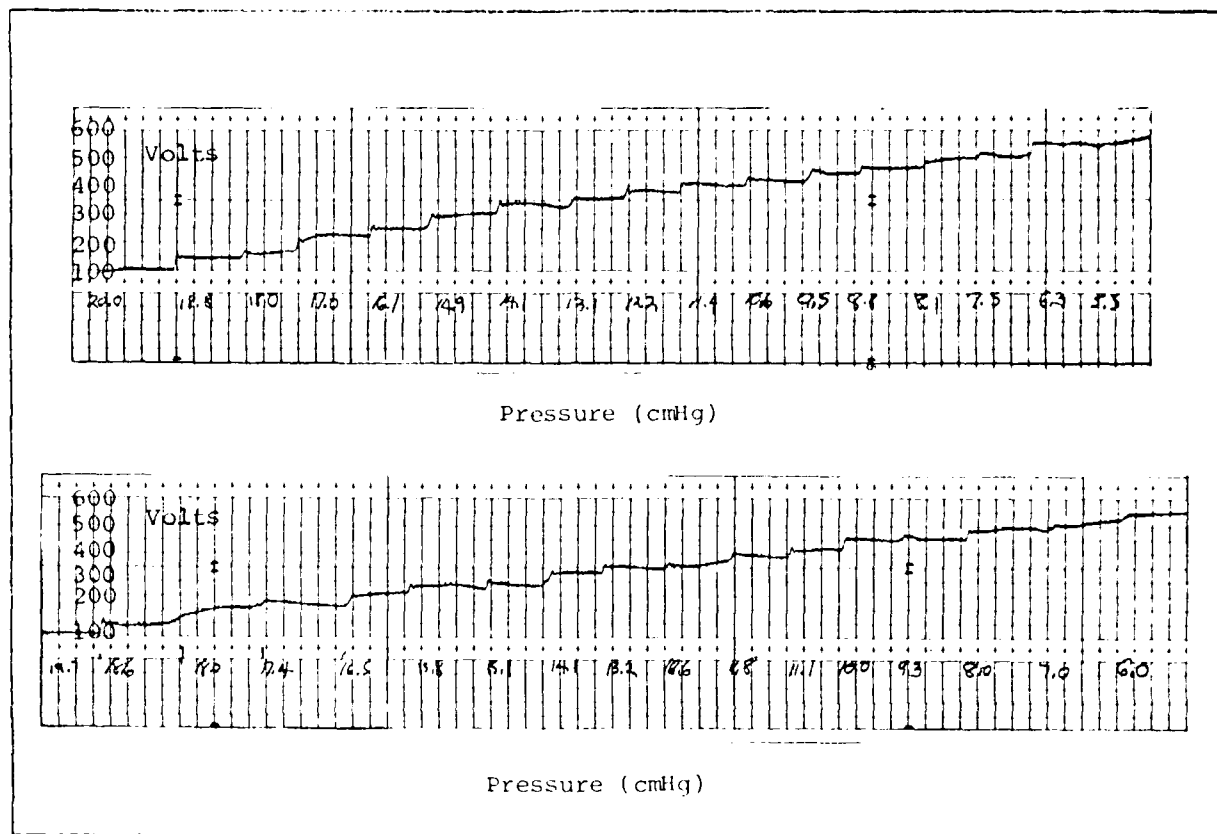
Figure 4.3   Pressure Data

The pressure data shown in Figure 4.3 was taken by applying a known pressure from the manometer to the diaphragm and measuring the voltage necessary to maintain the phase lock. The graph ranges from 100 to 600 volts with each vertical division representing 50 volts.
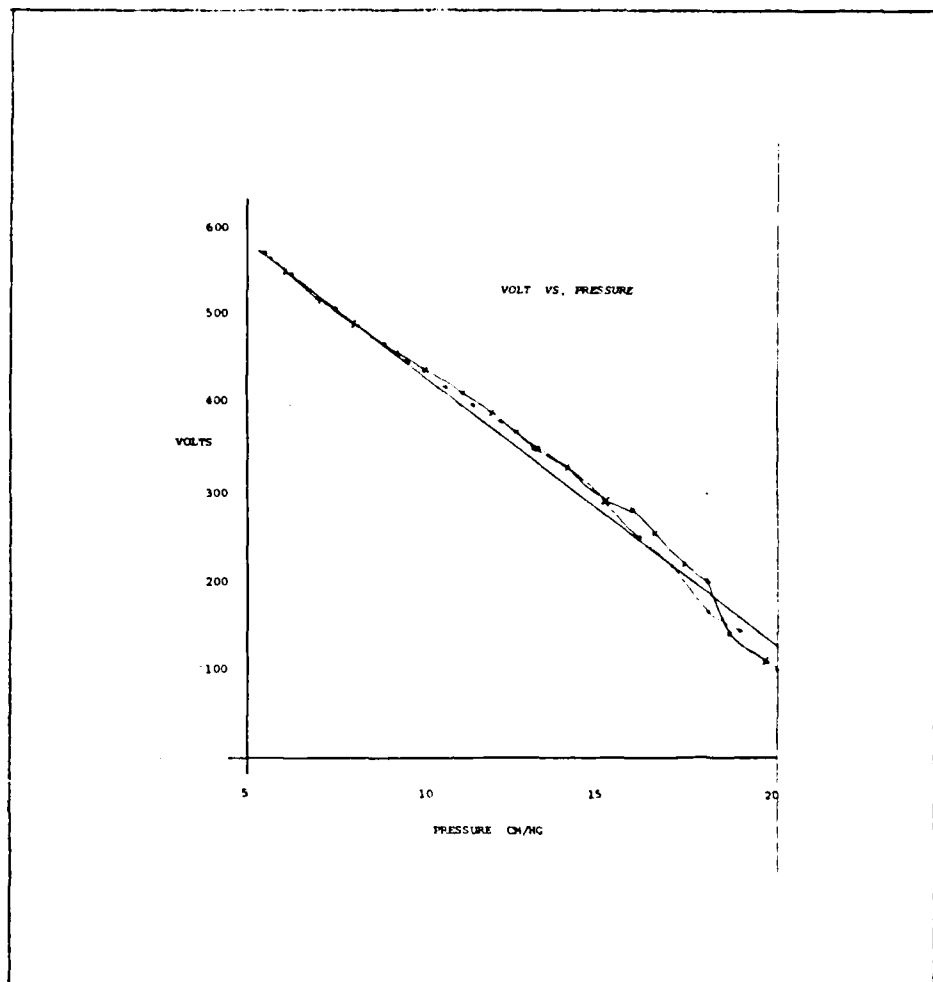
Figure 4.4   Graph of Pressure Data

This pressure data was then put in graphical form in Figure 4.4. The graph drops from left to right since the pressure on the diaphragm was pumped to a maximum value before the system was locked. The pressure was then released to take the readings. Nonlinearity at higher pressures is evident from the graph.

Computer Noise Analysis. The noise analyzer shown in Figure G.4 simplified the identification of noise sources. The photodiode was analyzed without an input to determine what noise power level was present. The power spectral density (PSD) of the photodiode without an input is shown in Figure 4.5. The frequency ranges from 0 to 5 KHz full scale is set by the computer to be 8×10^{-5} volts^2. Each major vertical division represents 16 db below the full scale value. This indicates photodiode noise is better than 50 db below the signal peak.

The power specral density of the locked system is the top graph in Figure 4.6. Multiple sample points (256) were taken and averaged to insure accuracy of the data. Full scale is set to 1.6×10^{-2} volts^2.

The lower graph of Figure 4.6 is the PSD of the system with the compensation network and the lock-in amplifier disconnected. This graph represents the noise contribution from the PZT and the HVA. The graph was intentionally lowered five small blocks on the paper to avoid overlap. The close resemblance of the two graphs indicates that the PZT and the HVA are the primary noise sources limiting system resolution. This assumes that the short term drift problem is correctable with design modifications.

The experimental preperation, procedures, and alignment lead to the gathering of data on drift, linearity, resolution, and noise for the fiber optic pressure transducer prototype. The results obtained form the basis for the conclusions and recommendations of Chapter Five.
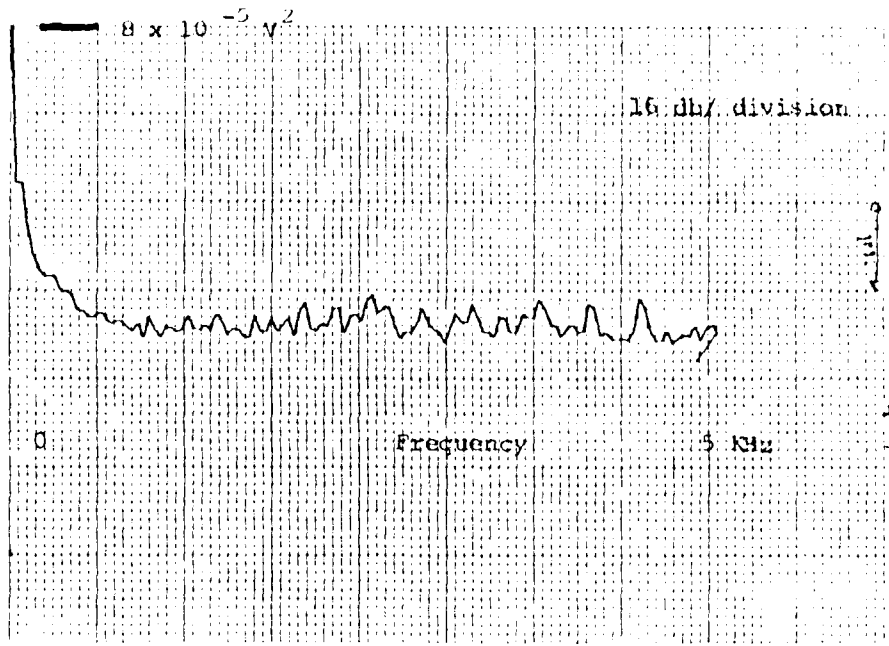
Figure 4.5 Photodiode Power Spectral Density (PSD)
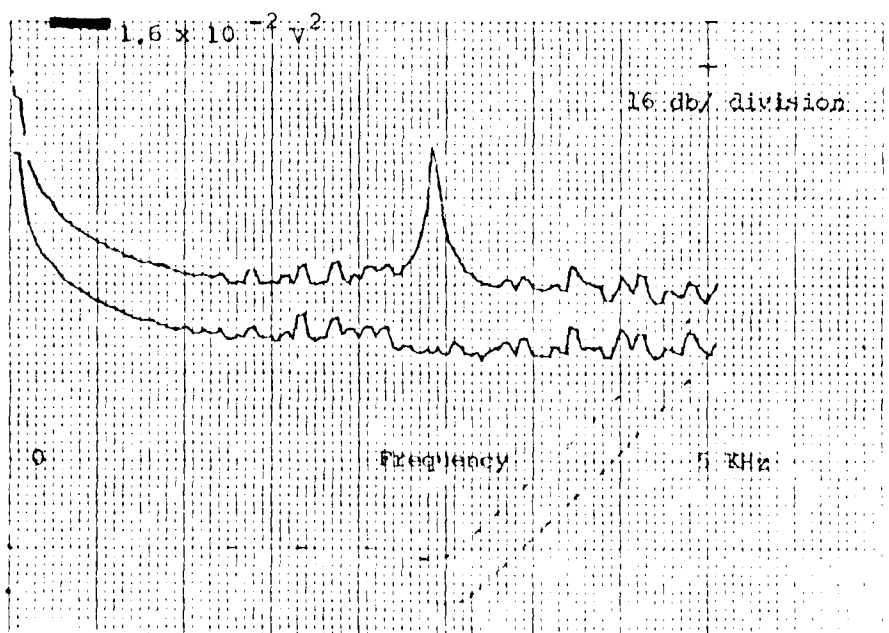

Figure 4.6 System PSD and PZT-HVA PSD

V. Conclusions and Recommendations

Conclusions

The goal of this research was to design, build, and test a prototype of the fiber optic pressure transducer to determine if the underlying principles were sound. Feasibility for use as an intravascular pressure sensor is considered.

Coherent light was efficently coupled into the single mode fiber core. It was shown that this laser light could be recaptured from the diaphragm in large enough quantities to permit the system to be phase locked with the PZT control system. The system operated as Planned.

Pressure measurement resolution was limited to 7 mmHg by the short term drift variations. Long term drift was negligible. The pressure range was limited to 150 mmHg by the scanning range of the PZT and the HVA. Selection of a different voltage to pressure scale factor would change this to any desired range.

Computer noise analysis indicated that the PZT and the HVA were the major noise sources limiting system resolution. Neglecting short term drift, resolution is limited to 3 mmHg by electronic noise.

The possibility of using an acousto-optic modulator for increased resolution and increased frequency range was displayed mathematically. This alternative was sought to replaced the noisier PZT apparatus.

The fiber optic pressure sensing technique was found to be a valid method to sense pressure variations. Noise limited the performance of prototype as would be expected for any new device. The system shows potential and continued research is warrented.

33

Recommendations

Many factors came into play during this thesis which suggest
alternative designs or alternative approaches to the problem of noise
reduction. The following recommendations should aid in the elimination
of identified inadaquacies. Recommendations will be made in the follow-
ing four areas: environmental, mechanical, electronic, and experimental.

Environmental. The inability to control temperature, air motion,
and vibrations added significantly to the noise present in the data.
The system rested upon four inches of foam in an effort to reduce
vibrations. A plexiglass cover was constructed to reduce air motion
and to help stabalize the temperature. The laser was inside the cover
which may have added to the problem since it is a heat source. The
system is very sensitive to any motion near the interferometer. This
suggests that the probe should be long enough so that it can be
removed from the area.

Mechanical. Stability of the mounting devices and the table plays
a large role in determining the noise level in the output data. The
arrangement as seen in Appendix G in the photo is far from ideal. The
mounts should be held rigidly to the plate without sloppy adjusting
mechanisms for alignment luxury. Miniaturization of components and the
distances between them is an effective way to reduce the noise level.
All of the optical components could be directly mounted to the same
plate in close proximity. The importance of stability cannot be over-
emphasized since the interferometer is easily capable of measurements
in the submicron region.

Electronic. The signal to noise ratio must be increased if the desired resolution is to be achieved. This can be accomplished by increasing the signal strength at the photodiode with a higher powered source or by increasing the coupling efficency to the fiber. Better mounting or focusing hardware could accomplish this task. The signal to noise ratio can also be increased by decreasing the noise level. The methods listed above can probably reduce the noise to get the desired 1 mmHg resolution. The PZT and the HVA must also be modified or replaced to get resolution below the 3 mmHg noise level. The alternate measurement method of Appendix F suggests one such possibility.

Experimental. Many improvements must be made before the fiber optic pressure sensor could be commercially useful. Besides the changes already mentioned, the diaphragms must be etched and mounted to the fiber to replace the bulky test mount used in this thesis. The alternate proposal of using an acousto-optic modulator is promising enough to warrant continued research in this area.

Summary. The prototype design represents the begining of this research effort. The pressure sensing technique was shown to be a valid approach. The prototype was shown to function as expected and to deliver impressive data considering this is the first attempt at building such a device. I beleive that the device could be used in the cardiovascular pressure sensing arena with only minor modifications. Many other applications exist where this device might be useful. Therefore, I recommend that research be continued in this area.

Bibliography

1. Benedict, Robert P. *Fundamentals of Temperature, Pressure and Flow Measurements.* New York: John Wiley & Sons, 1977.

2. Borky, John M. "Silicon Diaphragm Pressure Sensors with Integrated Electronics." Dissertation. School of Engineering, University of Michigan, Ann Arbor, Michigan, 1977.

3. Born, Max and Emil Wolf. *Principles of Optics.* New York: Pergamon Press, 1965.

4. Cobbold, R. S. *Transducers for Biomedical Measurements.* New York: John Wiley & Sons, 1974.

5. Fowles, G. R. *Introduction to Modern Optics.* New York: Holt, Rinehart and Winston, 1968.

6. Gardner, Floyd M. *Phaselock Techniques.* New York: John Wiley & Sons, 1979.

7. Giallorenzi, T. G. "Optical Communications Research and Technology: Fiber Optics," *IEEE Proceedings,* 66 (7): 744-780 (July 1978).

8. Grossman, W. *Cardiac Catherization and Angiography.* Philadelphia: Lea & Febiger, 1974.

9. Guyton, Arthur C. *Textbook of Medical Physiology.* Philadelphia: W.B. Sanders Company, 1976.

10. Hall, John "Monitoring Pressure with New Technologies," *Instruments and Control Systems.* 23-29 (April 1979).

11. Hecht, Eugene and Alfred Zajac. *Optics.* Reading Massachusetts: Addison Wesley, 1976.

12. Hocker, G. B. "Fiber Optic Measurement of Pressure and Temperature," *Applied Optics,* 18 (9): 1445-1448 (May 1979).

13. Hogg, R. D., A. H. Sanders, and F. A. Bick. "Biodynamic Angular Acceleration System." Project Report for Effects Technology Inc., Santa Barbara, California, 30 April 1980.

14. Holland, Charles R. and David J. Olkowski. "Evaluation of Errors in a Passive Ring Laser Gyroscope." MS Thesis, Wright Patterson AFB, Ohio: Air Force Institute of Technology, December 1978.

15. Hudson, M. "Calculation of the Maximum Optical Coupling Efficiency into Multimode Optical Waveguides," Applied Optics, 13 (5): 1029-1033 (May 1974).

16. Kabaservice, Thomas F. Applied Microelectronics. New York: West Publishing Co., 1978.

17. Kapany, N. S. Fiber Optics: Principles and Applications. New York: Academic Press, 1967.

18. Laser-Optics Short Course Notes, Air Force Institute of Technology, Wright Patterson Air Force Base, Ohio. Physics Department, June 1979.

19. Lindstrom, Lars H. "Miniaturized Pressure Transducer Intended for Intravascular Use," IEEE Transactions BME-17 (3): 207-219 (July 1970).

20. Michelson, A. A. Studies in Optics. Chicago: The University of Chicago Press, 1962.

21. Miller, S. E. Li, T. and E. A. J. Marcatili. "Research Toward Optical-Fiber Transmission Systems - Part I," IEEE Proceedings, 61 (12): 1703-1751 (December 1973).

22. Motes, Raymond A. "Compact Passive Laser Gyroscope Feasibility Investigation." MS Thesis, Wright Patterson AFB, Ohio: Air Force Institute of Technology, December 1979.

23. Murgo, Joseph P. and John P. Giolma. "Physiologic Signal Acquisition in a Clinical Cardiac Catherization Laboratory," IEEE Proceedings, 65 (5): 696-702 (May 1977).

24. Norton, Harry N. Handbook of Transducers for Electronic Measuring Systems. Englecliff, N. J. : Prentice Hall Inc., 1969.

25. O'Shea, Donald C., W. Russell Callen and William T. Rhodes. An Introduction to Lasers and Their Applications. Reading, Massachusetts: Addison Wesley, 1977.

26. Papoulis, Athanasios. Probability, Random Variables and Stocastic Processes. New York: McGraw-Hill Book Co., 1965.

27. Runyan, W. R. Silicon Semiconductor Technology. New York: McGraw-Hill Book Co., 1965.

28. Sanaur, Kensall D. Wise, and James B. Angell. " An IC Piezoresistive Pressure Sensor for Biomedical Instrumentation," IEEE Transactions BME-20 (2): 101-109 (March 1973).

29. Stillwell, john W. "A Feasibility Study of Single Mode Fiber Optic Evanescent Feild Coupling." MS Thesis, Monterey, California: Navel Post Graduate School, June 1979.

30. Webster, John G. Medical Instrumentation: Application and Design. Boston: Houghton Mifflin Co., 1978.

31. Wolf, Helmut F. Handbook of Fiber Optics. New York: Garland STPM Press, 1979.

32. Yariv, Amnon. Introduction to Optical Electronics. New York: Holt, Rinehart and Winston, 1976.

Appendix A: Silicon Diaphragm Etching Process

The diaphragm etching process used is well known and can be found in a number of microelectronics texts (Ref 16:48-50). Diaphragms are produced via the five step process shown in Figure A.1. Starting with a standard (100) orientation silicon wafer that has been properly cleaned, growth of a two micron thick silicon dioxide layer can be achieved by flowing steam across the wafer while it is in a 1200 °C furnace for a period of approximately five hours. Caution must be used to move wafers slowly into and out of the furnace to avoid thermal shock. Completion of this step will result in a SiO_2 layer as shown in Figure A.1.2.

A negative photoresist layer is now placed on the rough side of the wafer. The wafer is now exposed to ultraviolet light in the mask aligning unit. The mask used determines the size and quantity of diaphragms per wafer. After the photoresist is developed only the diaphragm area will be susceptible to the first etching step. This can be seen in Figure A.1.3.

Since both silicon and photoresist are impervious to hydraflouric acid (HF) they will not be attacked. But the SiO_2 will be removed from the diaphragm area in an orderly fashion, as seen in Figure A.1.4.

Now the wafer is submerged into a potassium hydroxide bath at 90 - 100 °C. A magnetic stirring capsule must be used to keep the H_2 bubbles away from the wafer or the process will stop. Potassium hydroxide removes silicon at a rate of one micron per minute leaving the diaphragm as shown in Figure A.1.5.

A.1.1

rough surface

Silicon wafer

mirror surface

(100) orientation

A.1.2

Silicon dioxide layer grown

2 microns thick

A.1.3

Negative photoresist added

and exposed in mask aligner

A.1.4

Silicon dioxide removed from

diaphragm area with HF acid

A.1.5

Silicon etched with KOH

to desired depth at rate

of 1 micron per minute.

now cut out diaphragms.
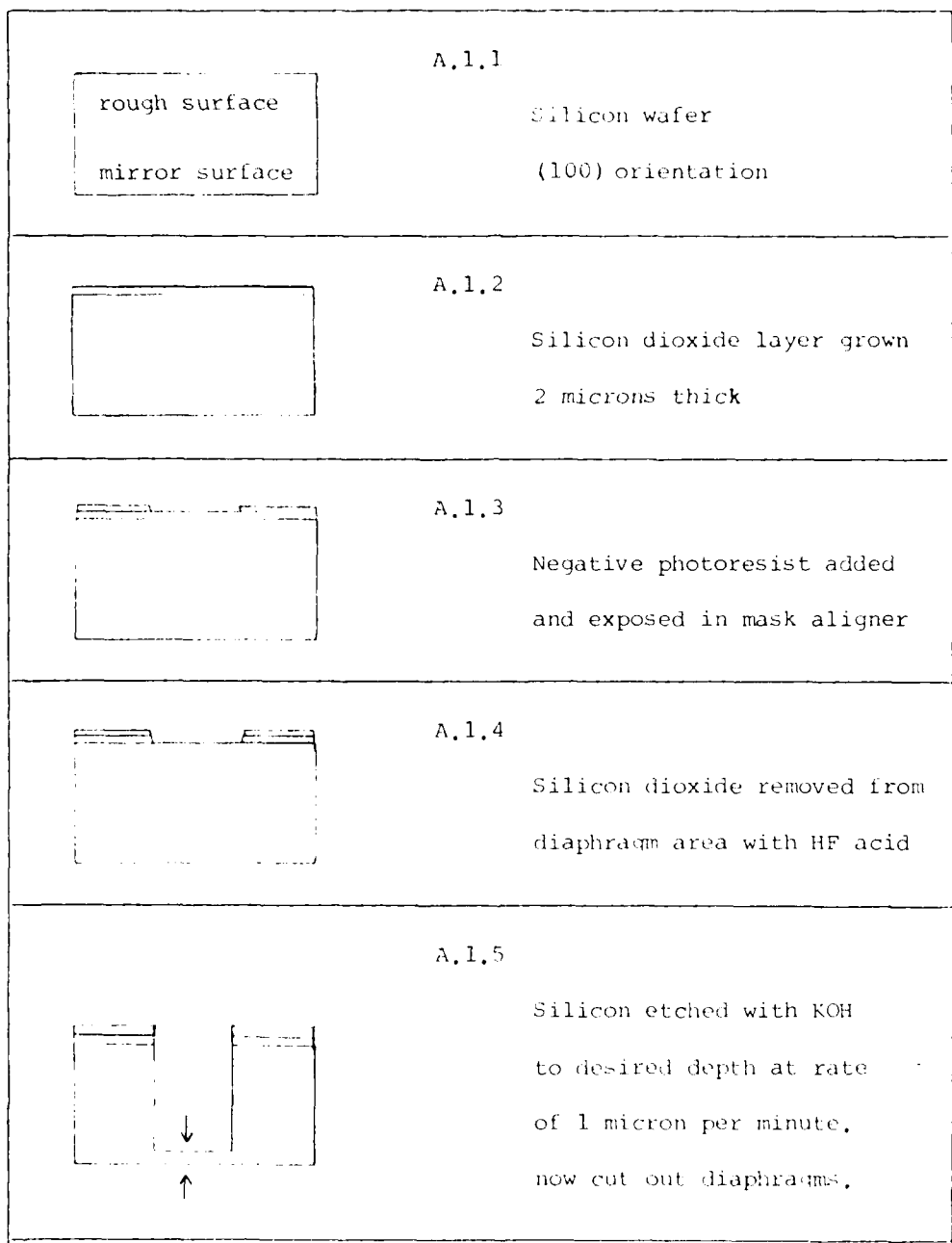
Figure A.1 Silicon Diaphragm Etching Process

The diaphragms can be taken down to a thickness of approximately 5 microns if desired. The diaphragms can now be cut out of the wafer and mounted appropriate to the application.

The diaphragm shown in A.1.5 has ideal thickness which is uniform over the whole diaphragm area with sharp corners at the edges. In reality, the degree to which the ideal case is achieved is dependent on etchant properties, crystal orientation, and control of process parameters. Isotropic etchants attack materials uniformly in all directions without reguard to crystal orientation. Anisotropic etchants, such as KOH, attack different orientations with different vigor. KOH was measured to attack the (100) plane 30 times faster than the (111) plane in silicon (Ref 2:58). This explains why KOH and a (100) orientation wafer was used to etch diaphragms in the above process. The depth of the wafer will be attacked 30 times faster than the sides. Figure A.2 shows what this will mean in diaphragm etching. Other parameters such as etchant temperature, hydrogen gas removal, and catalyst and etchant concentrations will effect results. The etching theory is covered in detail by Borky (Ref 2:57-76).

Isotropic Diaphragm

Anisotropic Diaphragm

Figure A.2   Isotropic Vs. Anisotropic Etching

The generation of an error signal used to drive the cavity length
to the resonance condition is based upon modulating the length of the
cavity such that the intensity of light out of the cavity is also
modulated dependent upon the length of the cavity relative to the
resonance condition.

If the intensity alone were used as an error signal, then the
variation of I from I_{max} would be an excellent indication of how far
the cavity must be moved to bring it into resonance. Unfortunately, that
signal alone is insufficient because there is no information to
indicate the direction in which the cavity length must be moved to
return it to resonance. By modulating the cavity at a frequency at
least a factor of two higher than the bandwidth required for the control
loop, an error signal can be generated which is both indicative of the
amount of error and the direction.

The method of operation can best be explained with reference to
Figure B.1. With the cavity such that it is in resonance with the
incident light frequency, the cavity would be in position A of the
figure. The modulation voltage V_m dithers the cavity length such that
the intensity detector output is as shown in Figure B.2. These two
signals are then mixed so that the output of the mixer (actually a
cross correlation detector) can be viewed as the product of the two
input signals. Thus the output of the mixer, called a phase sensitive
detector, is a sinusoidal in this case as shown in Figure B.2.
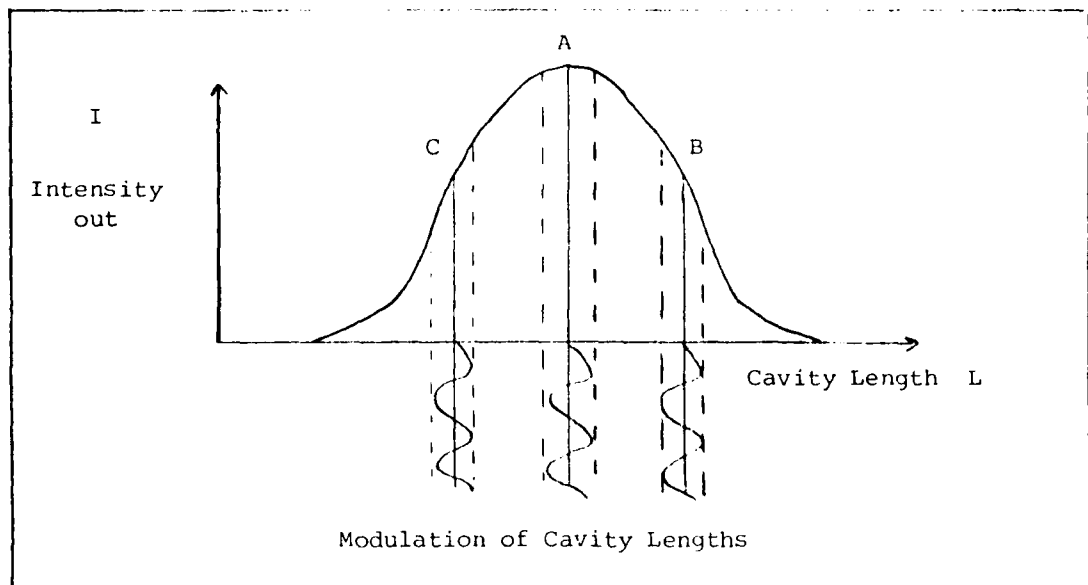
Figure B.1 Intensity vs. Cavity Length
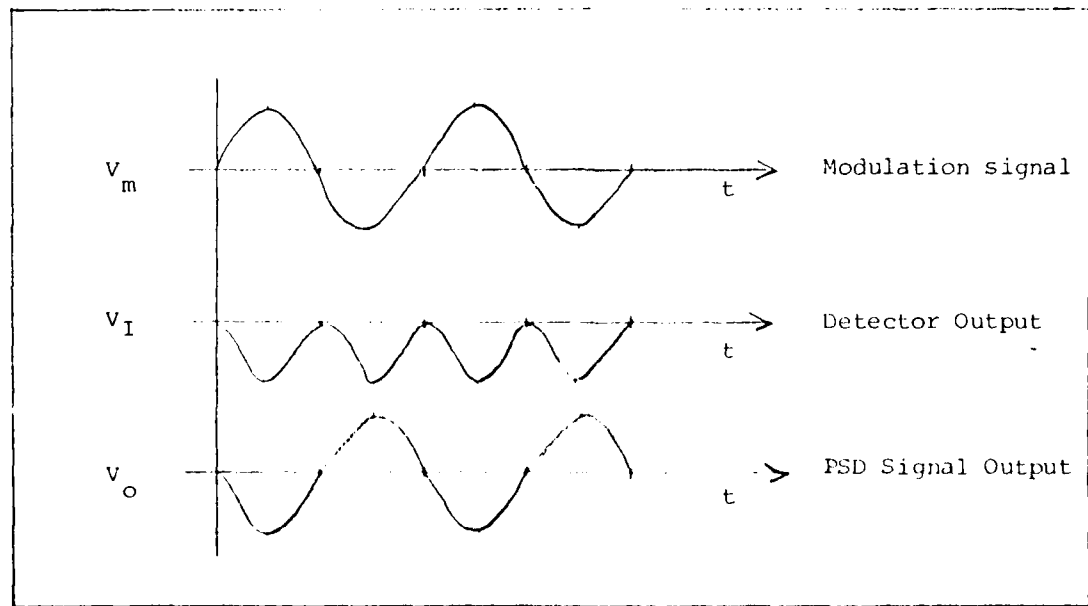
Figure B.2. V_m , V_I , V_o at Resonance L_r.

44

This signal is then low pass filtered to produce a zero DC level output indicating that the cavity is indeed on resonance.

For the case when the cavity is longer than required for the resonance condition refer to position B in Figure B.1. In this case the intensity detector output voltage is out of phase with the modulation signal and when multiplied produces a net negative signal as shown in Figure B.3. Again when low pass filtered, a negative voltage is generated indicating that the cavity must be shortened.

Finally, for the case when the cavity is shorter than required, the situation is as shown in position C of Figure B.1 and the phase sensitive output voltage is as shown in Figure B.4. The phase sensitive detedtor output voltage in this case is positive indicating a need to increase the cavity length.

The technique described here is used to monitor and correct for length fluctuations in both the PZT and alternative acousto-optic control loops.
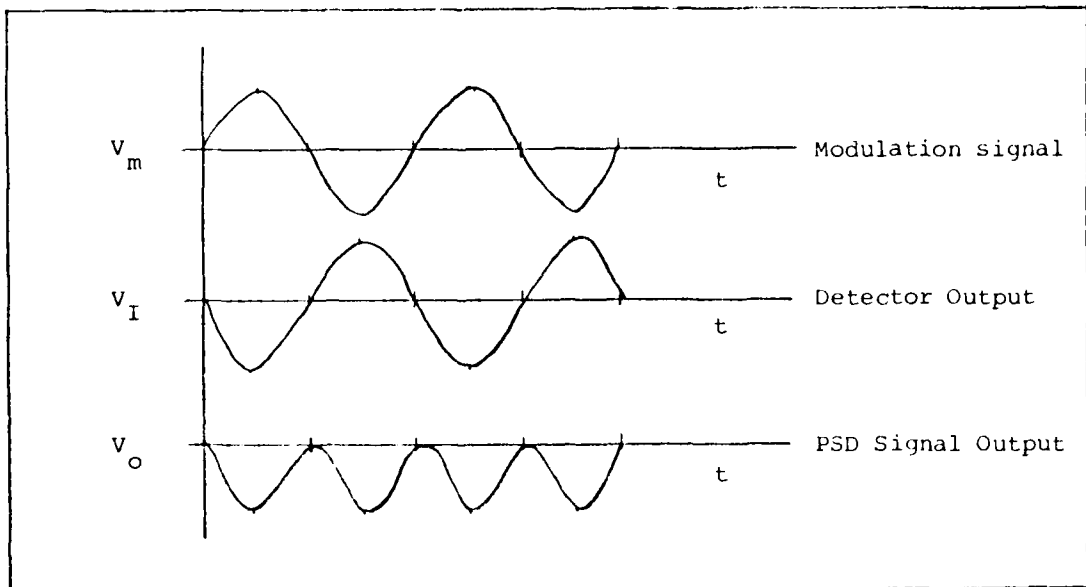
Figure B.3 V_m , V_I , V_o With Cavity Longer Than L_r
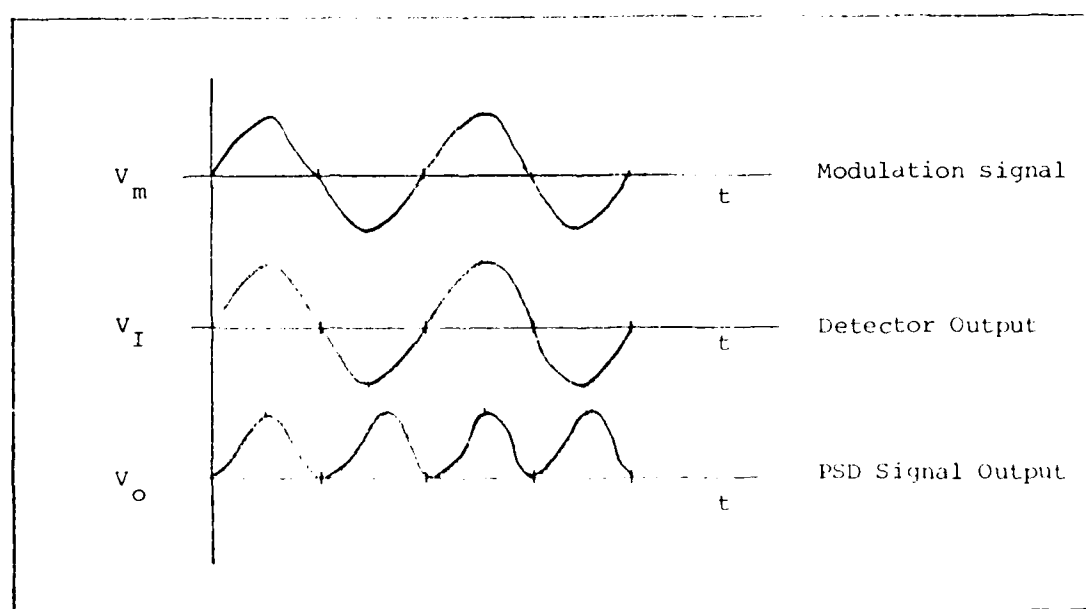
Figure B.4 V_m , V_I , V_o With Cavity Shorter Than L_r

46

Appendix C: Equipment Listing

The following equipment was common to both control loop methods.

Polished Silicon Wafers 1

Beam Splitter 1

Microscope Objective Lens, 5x, 10x, 20x . . . . 1 ea

Optical Fiber, Valtec BF-SM-632 Single Mode 1

Fiber Translator, NCR FP-1 1

Photodiode, United Detector PIN-6DP 1

Photodiode Circuitry (Figure D.1) 1

Compensator Circuitry (Figure D.2) 1

Lock-In Amplifier, Princeton Applied Research Model 124A . . . 1

Compensator Power Supply, Hewlett Packard Model 6205B 1

Chart Recorder 1

Neutral Density Filter, Focusing Lens, Aperature . . . . 1 ea

Mounting Hardware (From AFIT Shop) . . . .

The following equipment is associated with the PZT control loop.

Laser & Supply, Spectra Physics Model 142 . . . . 1 ea

High Voltage DC Op-Amp, Burleigh PZ-70 1

PZT Aligner Translator, Burleigh PZ-80 1

PZT Translator Mount 1

47

The following equipment is associated with the A/O control loop.

Modified Laser Exciter, Spectra Physics Model 132 1

Gain Tube, Jodon cf-16.1-1.5 1

Dielectric Mirrors, Flat 100%, Curved 99% . . . . 1 ea.

Acousto-optic Modulator, Coherent Associates Model 305 1

Signal Generator, Hewlett Packard Model 8640B 1

Wideband Amplifier Module, R.F. Power Labs Model M3058 1

WAM Power Supply, Trygon Electronics H36-30A 1

The following Equipment was used for spectral analysis.

Scanning Interferometer Driver, Spectra Physics Model 476 . . 1

Interferomter Spectrum Analyzer, SP Model 470 1

Photodiode, Spectra Physics Model 471 1

Mount, Spectra Physics Model 381 1

The following equipment was used for noise analysis.

PDP 11/15 Computer 1

X-Y Recorder, Hewlett Packard Model 7034A 1

Control Unit/ Time Data, Model GR 1923 - 3000 1

Oscilloscope, Tektronics 1

Appendix D: Circuit Diagrams

Two alternative circuits are shown for the photodiode amplifier
in Figure D.1. The first uses an operational amplifier and the
second uses a nine volt bias battery. Figure D.2 shows the compensation
circuit used in the contol loop.
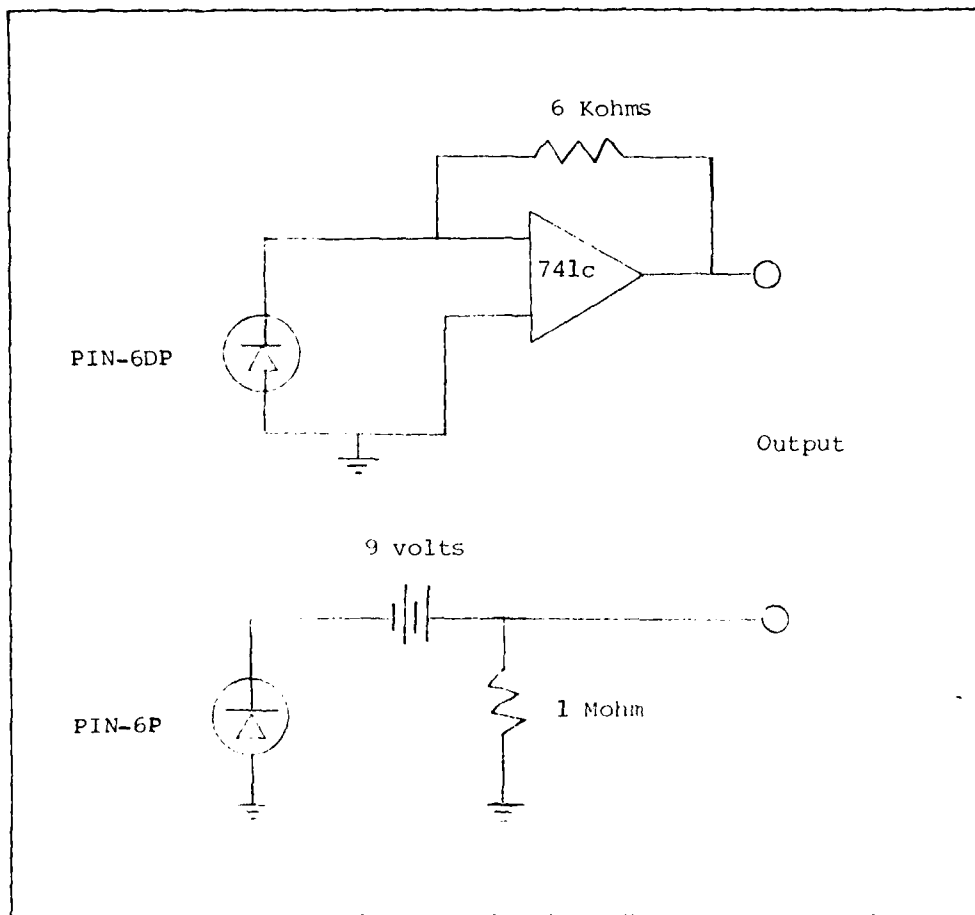
Figure D.1 Photodiode circuits
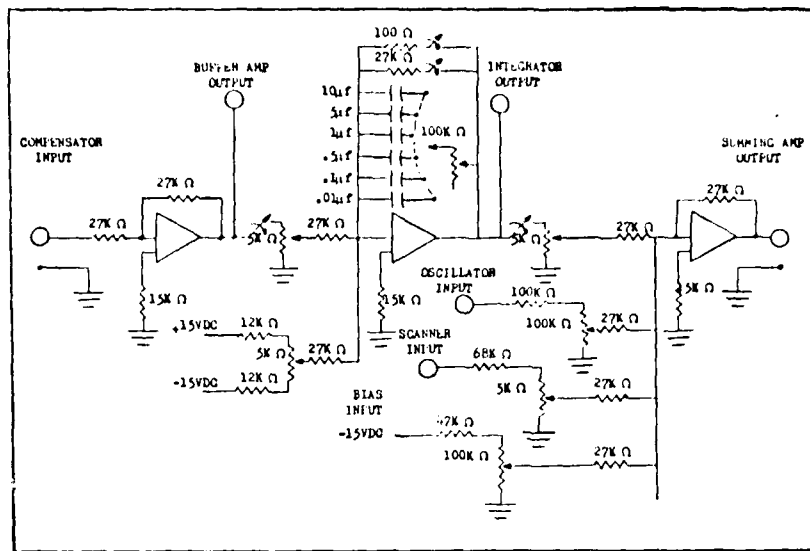
Figure D.2   Compensation Circuit

Appendix E: Biomedical Application

Numerous applications exist for the fiber optic pressure transducer. In order to structure this thesis investigation a particular biomedical application was adopted. The design constraints imposed by the in vivo cardio-vascular pressure sensor application were challenging and restrictive. Decisions concerning probe and diaphragm construction result from the limitations incurred from this application.

Advances in medical instrumentation have decreased the complexity of the modern physician's task in many ways. But the physician must keep abreast of advancing technology before true gains are realizible. Cardiologists have known the value of cardio-vascular pressure measurements for many years. "Cardiac catherization is performed in virtually all patients in whom heart surgury is contemplated. This procedure yields information that may be crucial in detining the timing, risks, and anticipated benefit for a given patient". (Ref 30:367) The information gathered via a pressure sensor in the catherization process has decreased the complexity of the cardiologist's task by giving him more information upon which to base his decisions. The process is far from perfected. Pressure transducers need to be designed to better fulfill these needs.

Current transducers have many limitations and often yield only part of the desired pressure data. It has been speculated that more information exists than current transducers have the ability to see. So, more precise transducers need to developed to meet these needs.

51

"It is hoped that more precise identification of disease conditions will be possible ... by preserving details of the fine structure of the pressure waveforms in the heart and the adjacent vessels. This is based on the beleif that such factors as damage from infarction, incomplete valve closure, interchamber fistulas, and so on will have identifiable signitures in the form cf turbulence or perturbation of the normal pressure contour." (Ref 2:7-8)

The significant limitations of the currently used catheter manometer system can be over come by mounting the transducer at the end of the sensing probe and eliminating the hydraulic connection. Many of the new electronic sensors have been used in this way. But all presently used transducers have serious problems of their own. They have all in some way been unable to meet the following criteria for an acceptable intravascular pressure transducer, from Borky and Webster.

Sensor Criteria

1. Accuracy and Linearity of $\pm$ 1% from 0 to 250 mmHg with resolution better than 1 mmHg.

2. Temperature compensation if necessary over the range from 30°C to 45°C.

3. Sensor diameter of 1mm maximum to allow use in pediatric patients.

4. Patient safty must be a primary concern.

5. Absolute pressure reading is required.

6. Easy or infrequent calibration of equipment.

7. Sensor must be durable in a hospital environment.

8. Sensor must be cost effective.

Cardiac Catherization

Cardiac catherization is a process by which intravascular blood pressure readings can be taken. A catheter is nothing more than a small diameter rubber hose that can be inserted into the body through an orafice or an artificial opening. In the case of cardiac catherization this hose enters a vein or artery and is guided to the heart region using fluoroscopy. This form of positioning allows pressure measurement in all four chambers of the heart and in the surrounding vessels. During catherization ectopic beats and cardiac fibrillation occur frequently. Therefore personnel and equipment must be on hand to restart or correct the heart's fluctuations. Other readings taken concurrently are cardiac output, blood and respiratory gases, blood oxygen saturation, and metabolic products monitoring. Radiopaque dyes are also used frequently to veiw heart motion. Research has been accomplished using balloon tipped catheters to eliminate the need for fluoroscopy techniqes. In this case the blood flow takes the sens   the desired area.

Current Cardiac Pressure Sensors

Many different transducer schemes have been used to obtain - the valuable cardiac pressure information. The most commonly used is the catheter manometer because of its simplicity and low cost. Another system that is making significant headway is the electric strain gage. Another system of interest due to some similarities to this thesis is the optical intensity sensor. Each of these systems

will be discussed in depth. Other ideas which have been given

consideration in this application are: variable capacitance,

variable inductance, piezoelectric, piezoresistive, linear variable

differential transformer, and semiconductor devices.

Catheter Manometer

The catheter manometer as shown in Figure E.1 is a simple

hydraulic system that couples cardiac pressure outside the body to

a manometer where it can be read. The advantages of this system are

its simplicity and its low cost. The performance of the catheter

manometer could best be described as sometimes adaquate. The system

has many problems that have led to vast research in the area in an

attempt to find a replacement that offers significant improvement.

The blood pressure is coupled outside the body via a sterile saline

solution inside the catheter. Frequent cleaning may be necessary to

remove the blood clots that form at the hose opening. The frequency

response of the system changes drastically with the hose diameter.

A hose diameter in excess of 2 mm is usually used and this causes

increased risk to the patient. Pediatric patients are often too small

to permit pressure readings to be taken by this method.

The accuracy of the catheter manometer system is very poor.

Air bubbles form in the fluids involved and become compressible

leading to some of this inaccuracy. The size of the catheter causes

interference with the blood flow and changes readings. The hydraulic

system itself limits the frequency response by acting like a filter.
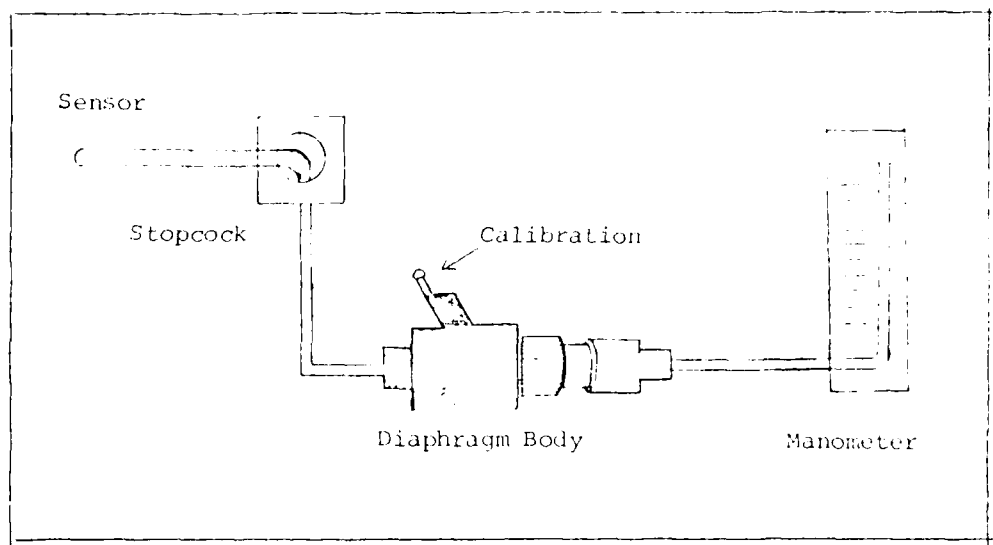
Figure E.1   Catheter Manometer   (Ref 30:337)

Electric Strain Gage

Unlike the catheter manometer the strain gage as shown in
Figure E.2 is an intravascular system, meaning that the transducer
is contained in the tip of the sensing probe. The strain gage
contains a diaphragm that senses the pressure and moves an armature
that is connected to two sets of strain gages set up in a Wheatstone
bridge configuration. The pressure applied to the diaphragm is
directly related to the degree of inbalence created in the bridge
network. Therefore an electric output will occur when a pressure is
applied. Even though strain gages are more accurate than the
catheter manometer system they are used less frequently.

Strain gage probes have many serious problems. The probes are
costly to build in a size compatible with this application. The

65

smallest probe size available as of 1978 was F5 catheter (1.67 mm).
Other problems include temperature drift, electrical drift,
fragility, and the inability to withstand sterilization. Also
some research has been done that indicates that electrical currents
within the strain gage probe may be responsible for increased
fibrillation attacks in patients.
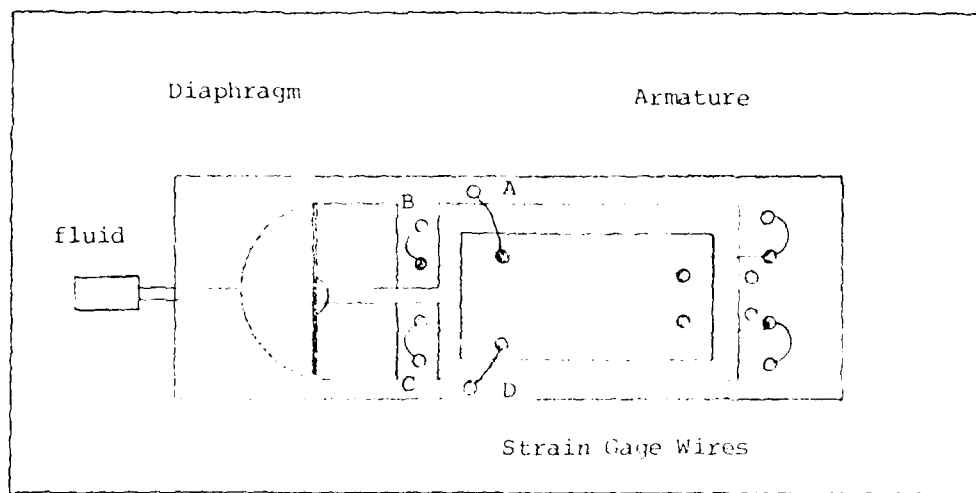
Figure E.2 Electric Strain Gage (Ref 30:337)

Optical Intensity Sensor

The transducer displayed by Lindstrom (Ref 19:208) measures
light intensity reflected from a moving membrane. Light is coupled
into a fiber bundle as shown in Figure E.3 and then it is reflected
back down different fibers. The reflective membrane changes in
curvature and in distance from the fiber bundle as pressure is

applied. A relationship was then developed between the amount of light received at the detector and the pressure on the membrane. Measurements indicate linearity of 2.5% over the desired pressure range. Sensitivity is a major problem with this system as indicated in the article. Other problems include temperature sensitivity and size. Although the size could be reduced if an attempt were made. Some similarities do exist between this system and the fiber optic system that is the focus of this thsis but they are slight.
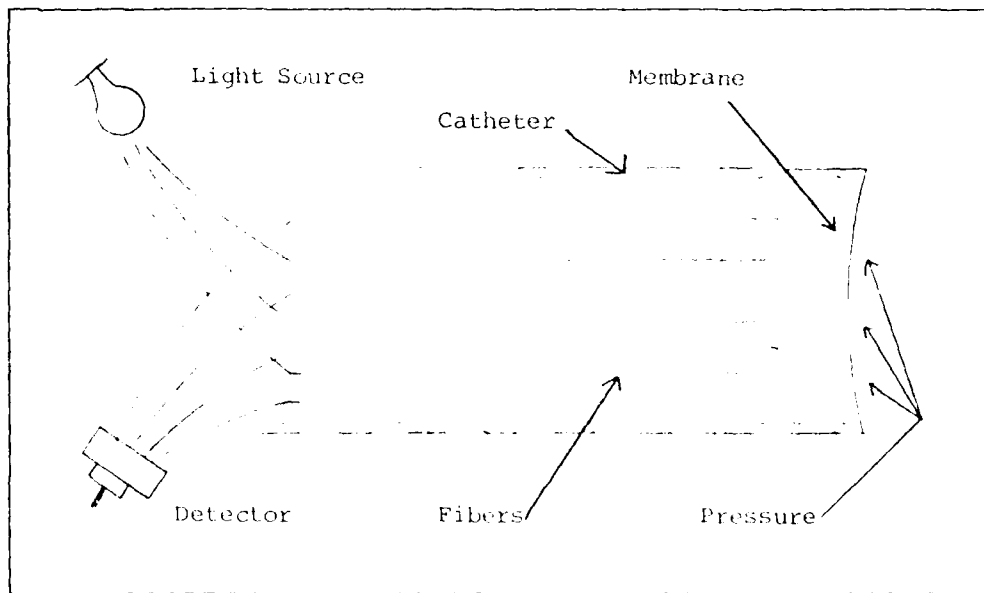

Figure E.3   Intensity Sensing Transducer   (Ref 19:208)

Appendix F: <u>Alternate Measurement Method</u>

General Description

The active element of the PZT control loop is replaced in this

approach by an acousto-optic modulator. The acousto-optic modulator

changes the frequency of the laser beam by Bragg diffraction from an

acoustic wave. This in turn changes the optical path length in terms

of the number of wavelengths between the beam splitter and the diaphragm

mirror. The two legs of the interferometer must be considerably different

in length for this approach to work. This hints that a single mode

laser will be required to obtain phaselock and a useable pressure

range. The coherence length of a normal laboratory HeNe laser (30 cm)

is not great enough for this system to function usefully. The acousto-

optic modulator offers two advantages over the PZT. First, the output

variable is frequency instead of voltage and this when coupled with

the superior electronics associated with the acousto-optic modulator

suggests significant improvements in resolution. Secondly, the frequency

response of the acousto-optic is not limited by its mechanical inability

to respond to high frequency inputs. Therefore, the frequency response

is expected to be much better than the 2 KHz displayed by the PZT

method.

The operation of the acousto-optic modulator system can be seen

easily from Figure F.1. The Michelson interference pattern is locked

using the same modulation technique as shown in Appendix B. The output

variable is the frequency of the voltage controlled oscillator (VCO).
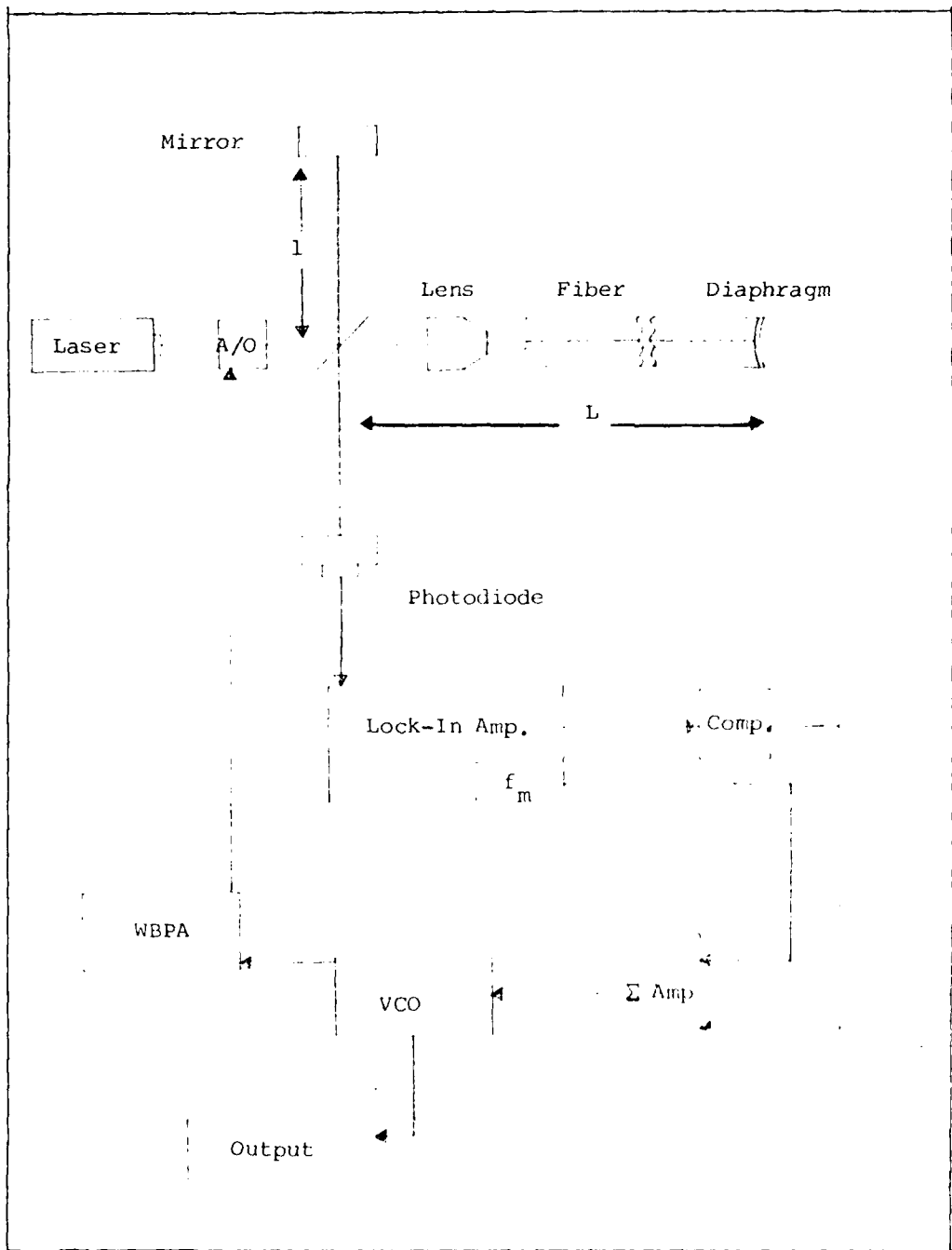
Figure F.1 Acousto-Optic Modulation Method General Diagram.

The intensity of the interference pattern is converted to an electrical signal by the photodiode. The input signal determining the VCO output is determined by summing f_m (constant 50 KHz) and the phase information contained in the compensated lock-in amplifier signal. The output of the summing amplifier is a voltage level that stores the initial phase relationship and drives the VCO to maintain that phase. The VCO changes the FM modulation frequency sent to the acousto-optic modulator that in turn changes the laser frequency. The wide band power amplifier merely supplies the correct power requirements of the acousto-optic modulator.

Acousto-Optic Modulation

Acousto-optic modulation offers a convienient means to control frequency, intensity, or direction of a laser beam. The principle relies upon Bragg diffraction of light by acoustic waves (up to 10^{10} Hz). The acoustic wave is a sinusoidal pertibation of the materials density. As the density changes so does the index of refraction. Therefore its usefullness as a variable frequency moving mirror is realized. The motion of this mirror is the factor giving rise to the doppler frequency shift in the refracted laser output beam. Specifications indicate that 50 percent cr better of the laser power can be shifted into the first shifted dot. The equations relating this efficiency can be found in Yariv. (Ref 32:346)

Pressure Vs. Frequency Equation

An equation needs to be derived relating frequency and pressure to better understand system operation. The diaphragm equation displayed

In chapter two (Eq. 2.5) relates the change in length (ΛL) to the change in pressure (δP). These two equations can then be combined to yeild a relationship between pressure change and the necessary frequency change (Λf) to maintain phaselock.

Recall that the phaselock control loop locks the signal and thus maintains a constant number of wavelengths over the region (L-1). This is accomplished by changing the wavelength of the laser light slightly with the acousto-optic modulator. This fact leads to the following equation for frequency change.

$$\Lambda f = f_t - f_k$$

where: Λf = FM modulation range of VCO driving A/O.
         f_t = Total laser frequency after modulation.
         f_k = Laser frequency plus A/O cnter frequency.

since $c = \lambda f$

$$\Delta \lambda = \lambda_t - \lambda_k = c/f_t - c/f_k = - \frac{c \, \Lambda f}{f_t \, f_k}$$

where: $\Delta \lambda$ = Change in wavelength due to Λf.

This change in wavelength causes a change in optical path length (ΛL) of $n\Delta\lambda$ where n is the number of wavelengths affected.

$$n = \frac{2 \, (L - 1)}{\lambda_t}$$

so:

$$\Lambda L = n \, \Delta \lambda = - \frac{2 \, (L - 1) \, c \, \Lambda f}{\lambda_t \, f_t \, f_k}$$

which reduces to:

$$\Lambda L = - \frac{2 \, (L - 1) \, \Lambda f}{f_k} \qquad \text{(Eq. F.1)}$$

Recall that (Eq. 2.5) shows the length change to be equated to the differential pressure applied to the diaphragm as follows.

61

$$\Lambda L = 8.425 \times 10^{-14} \ \frac{R^4}{t^3} \ \delta P$$

Equating these two formulas yeilds the following result.

$$\Lambda f = - \frac{8.425 \times 10^{-14} R^4 f_k \ \delta P}{2 (L - 1) t^3}$$

Setting $f_k = 4.74 \times 10^{14}$ Hz (for a HeNe laser) yeilds the simplified formula below.

$$\Lambda f = - \frac{20}{(L - 1)} \ \frac{R^4}{t^3} \ \delta P \qquad \text{(Eq. F.2)}$$

where: Λf = VCO modulation frequency in Hz.
   L = Length of interferometer sensing branch in cm.
   1 = Length of interferometer reference branch in cm.
   R = Diaphragm radius in cm.
   t = Diaphragm thickness in cm.
   δP = Differential pressure in dynes/cm^2.

Each of the parameters in (Eq. F.2) have unseen limitations that drastically effect the usefulness of the system. The modulation frequency (Λf) is equipment limited to 640 KHz for the equipment shown in Appendix C. The length difference $(L - 1)$ is restricted to be less than the coherence length of the laser in order to permit interference of the two beams. The minimum diaphragm thickness (t) is limited to 5 microns by the etching technique shown in Appendix A. But the thickness is also limited by the linearity assumption made in chapter two. $\Lambda L_{max} < t/4$ This assumption guaranteed linearity better than 1% for the diaphragm. Table F.1 shows the limitations and the possible values for the radius to thickness ratio (R^4/t^3). Close analysis of these parameters shows that not all can be satisfied with a multimode laser source.

The necessary laser coherence length can be determined from the

Thickness (microns)	5	50	100	300
Radius (cm)				
.01	80	.08	1×10^{-2}	3.7×10^{-4}
.1	8×10^{5}	8×10^{2}	1×10^{2}	3.7
1	8×10^{9}	8×10^{6}	1×10^{6}	3.7×10^{4}
10	8×10^{13}	8×10^{10}	1×10^{10}	3.7×10^{8}

Table F.1   Calculated Values for R^4/t^3.

following essential conditions. The drift data shown in chapter four

indicate that thermal and mechanical noise of the environment limit

length (ΔL) resolution to approximately $\lambda/10$ or .06 microns. Therefore,

to obtain 1 mmHg resolution over the range 0 - 250 mmHg as indicated

in the Biomedical criteria in appendix E the maximum length change (ΔL_{max})

due to 250 mmHg must be 25 λ or 15 microns. Solving equation 2.5 for

these conditions indicate the need for $R^4/t^3 = 5.4 \times 10^3$. With the

desired radius of R = .5 mm the diaphragm thickness must be t = 105

microns. Plugging the appropriate values into equation F.2 shows the

laser coherence length needed assuming no improvents in system

electronics are acheivable. The necessary coherence length is L_c =

560 meters. This is not discouraging since two avenues of correction

exist. A special application VCO could be built with an extended FM

modulation range to correct the problem. Also a single mode laser

could be acquired with the necessary coherence length.

Testing done with the acousto-optic modulator and single mode
fiber indicate that the VCO FM modulation range could be increased by
a factor of 20 to 12.5 MHz and still keep the shifted beam within the
5 micron core of the fiber. This improvement alone would reduce the
required coherence length of the laser to 28 meters. The expanded
VCO range permits a tradeoff for fiber probe length. The probe can
be as short as 28 meters or as long as the coherence length of the
laser. For long fibers, loss mechanisms within the fiber can no
longer be ignored. Scattering mechanism within the fiber may well
be the limiting case.
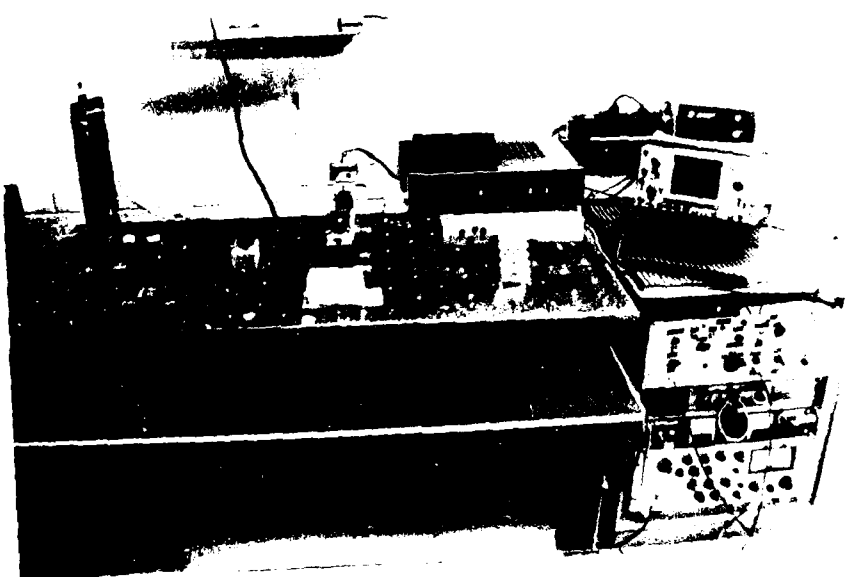
Figure G.2 Fiber Mounting Apparatus

The diaphragm pressure mount is shown in Figure G.3. The diaphragm
mount allows pressure to be applied to the back of the silicon
diaphragm by pumping up the mercury manometer. The arm attached to
the top of the mount holds the fiber firmly near the mirror surface.
A small gap exists between the fiber and the mirror to permit flexing
of the diaphragm. The radius of the diaphragm can be adjusted by
changing the washers that hold the wafer in the mount. This allows
the scale factor of the pressure sensor to be varied.

Figure G.4 shows the GR noise analysis computer with the X-Y
plotter.
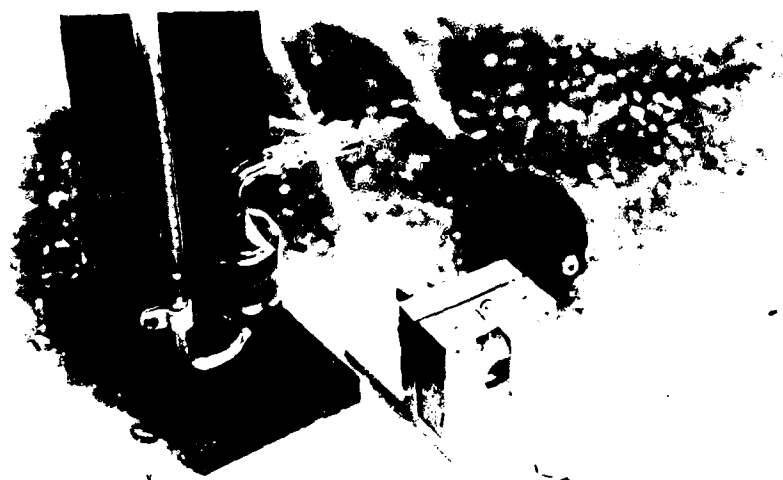
Figure ... Equipment Pressure Plate

Figure ...

VITA

Eddie J. Preston was born on 27 December 1954 in Alamagordo, New Mexico. He graduated from Adrian High school in Adrian, Michigan in 1973. He entered into the USAF and was trained as a radar technician (AN/FPS-85) at Keesler AFB Mississippi. He worked one year with the 20th Surveillance Squadron at Eglin AFB before accepting an ROTC scholorship at the University of Michigan in 1975. He received the degree of Bachelor of Science in Electrical Engineering and his commission into the USAF on 28 April 1979. He is currently working on the degree of Master of Science in Electrical Engineering at the Air Force Institute of Technology. He has been selected for the Electronic Communications Officer (3055) training program at Keesler AFB to begin 20 January 1981.

Permanent Address: 2082 Sword Hwy.
Adrian, Mich. 49221

REPORT DOCUMENTATION PAGE	READ INSTRUCTIONS BEFORE COMPLETING FORM

1. REPORT NUMBER	2. GOVT ACCESSION NO.	3. RECIPIENT'S CATALOG NUMBER
AFIT/GE/EE/ 81M-7	AD A100 886	

4. TITLE (and Subtitle)	5. TYPE OF REPORT & PERIOD COVERED
PRESSURE SENSING WITH FIBER OPTICS AND INTERFEROMETRY	MS THESIS
	6. PERFORMING ORG. REPORT NUMBER

7. AUTHOR(s)	8. CONTRACT OR GRANT NUMBER(s)

9. PERFORMING ORGANIZATION NAME AND ADDRESS	10. PROGRAM ELEMENT, PROJECT, TASK AREA & WORK UNIT NUMBERS
Air Force Institute of Technology (AFIT-EN) Wright-Patterson AFB, Ohio 45433	

11. CONTROLLING OFFICE NAME AND ADDRESS	12. REPORT DATE
	December, 1980
	13. NUMBER OF PAGES
	81

14. MONITORING AGENCY NAME & ADDRESS (if different from Controlling Office)	15. SECURITY CLASS. (of this report)
	UNCLASSIFIED
	15a. DECLASSIFICATION DOWNGRADING SCHEDULE

16. DISTRIBUTION STATEMENT (of this Report)

Approved for public release; distribution unlimited

17. DISTRIBUTION STATEMENT (of the abstract entered in Block 20, if different from Report)

18. SUPPLEMENTARY NOTES

Approved for public release; IAW AFR 190-17

FREDRIC C. LYNCH, Major, USAF   16 JUN

Director of Public Affairs

19. KEY WORDS (Continue on reverse side if necessary and identify by block number)

Pressure Transducer
Interferometry
Single Mode Fiber
Intravascular Blood Pressure Sensor

Phaselock Control
Acousto-Optic Modulation
Piezoelectric Length Transducer

20. ABSTRACT (Continue on reverse side if necessary and identify by block number)

A new pressure sensing device has been analyzed, built, and tested. The device uses a Michelson interferometer to monitor pressure-induced fluctuations of a polished silicon diaphragm. Probe flexibility is achieved by mounting the diaphragm on the end of a single mode optical fiber; the coupling apparatus used permits interference to occur with the fiber in one leg of the interferometer. The phase of the resulting

DD FORM 1473   EDITION OF 1 NOV 55 IS OBSOLETE   UNCLASSIFIED

pattern is locked using a piezoelectric length transducer and phaselock loop control techniques.

Formulas developed to model the system input/output characteristics led to the construction of a working prototype. Long term drift for the system was negligible. Short term drift limited the resolution of the system to 7 mmHg over the region 50 mmHg to 200 mmHg. The limited range resulted from the scanning limit of the piezoelectric length transducer. System linearity was approximately 5 percent. Computer noise analysis identified the high voltage DC amplifier and the piezoelectric length transducer as limiting resolution to 3 mmHg.

Acousto-optic modulation was examined as an alternative control method. This approach offers better resolution and better frequency response.

The performance of the prototype pressure sensing system suggests that state-of-the-art specifications could be achieved by this method. Application for intravascular blood pressure measurement is discussed.

DATE
ILMED

8